140 (2022) 213073

Contents lists available at ScienceDirect

Biomaterials Advances

journal homepage: www.journals.elsevier.com/materials-science-and-engineering-c

Metronidazole nanosuspension loaded dissolving microarray patches: An engineered composite pharmaceutical system for the treatment of skin and soft tissue infection

Qonita Kurnia Anjani [a,b], Akmal Hidayat Bin Sabri [a], Juan Domínguez-Robles [a], Natalia Moreno-Castellanos [c], Emilia Utomo [a], Luki Ahmadi Hari Wardoyo [d], Eneko Larrañeta [a], Ryan F. Donnelly [a,*]

[a] School of Pharmacy, Queen's University Belfast, Medical Biology Centre, 97 Lisburn Road, Belfast BT9 7BL, UK
[b] Fakultas Farmasi, Universitas Megarezky, Jl. Antang Raya No. 43, Makassar 90234, Indonesia
[c] Basic Science Department, Faculty of Health, Universidad Industrial de Santander, Bucaramanga 680001, Colombia
[d] Fakultas Seni Rupa dan Desain, Institut Teknologi Bandung, Jl. Ganesa No.10, Bandung 40132, Indonesia

ARTICLE INFO

Keywords:
Metronidazole
Soluplus®
Dissolving microarray patches
Skin and soft tissue infections

ABSTRACT

Bacteroides fragilis is one of the most common causative group of microorganisms that is associated with skin and soft tissue infections (SSTI). Metronidazole (MTZ) is the drug of choice used in the treatment of SSTI caused by the bacterium. However, owing to its physiochemical properties, MTZ have limited skin permeation, which render the drug unsuitable for the treatment of deep-rooted SSTIs. One strategy to overcome this limitation is to reformulate MTZ into nanosuspension which will then be loaded into dissolving microarray patches (MAPs) for the treatment of SSTIs caused by *B. fragilis*. Herein, we report for the first time on the preparation and optimisation of MAP loaded with MTZ nanosuspension (MTZ-NS). After screening a range of polymeric surfactants, we identified that Soluplus® resulted in the formation of MTZ-NS with the smallest particle size (115 nm) and a narrow PDI of 0.27. Next, the MTZ-NS was further optimised using a design of experiments (DoE) approach. The optimised MTZ-NS was then loaded into dissolving MAPs with varying MTZ-NS content. Furthermore, 3-(4,5-dimethylthiazol-2-yl)-2,5-diphenyl tetrazolium bromide (MTT) and cell proliferation assays along with LIVE/DEAD™ staining on the 3T3L1 cell line showed that the MTZ-NS loaded dissolving MAPs displayed minimal toxicity and acceptable biocompatibility. *In vitro* dermatokinetic studies showed that the MTZ-NS loaded MAPs were able to deliver the nitroimidazole antibiotic across all strata of the skin resulting in a delivery efficiency of 95 % after a 24-hour permeation study. Lastly, agar plating assay using bacterial cultures of *B. fragilis* demonstrated that MTZ-NS loaded MAP resulted in complete bacterial inhibition in the entire plate relative to the control group. Should this formulation be translated into clinical practice, this pharmaceutical approach may provide a minimally invasive strategy to treat SSTIs caused by *B. fragilis*.

1. Introduction

Skin and soft tissue infections (SSTIs) impose a substantial financial burden to health care systems, accounting for approximately 10 % of all hospitalized patients [1,2]. This group of infections are caused by invasion of bacteria and other microorganisms into the skin and underlying tissue. The condition may range from mild localised superficial infection, such as erysipelas, to more deep-rooted tissue infection, such as cellulitis [3]. The exact etiology of SSTI is multifaceted and may be caused by several microorganisms, ranging from virus, fungi and parasite with bacterial infection being the most prevalent cause [3–5]. One of the most common causative group of microorganisms associated with SSTIs is *Bacteroides fragilis* [6]. Transmission of *B. fragilis* and closely related bacteria general from normal mucosal location may arise as a result of trauma such as animal/human bites, burns, cuts, or penetration of foreign objects, including nosocomial infections which may arise

* Corresponding author at: Pharmaceutical Technology, School of Pharmacy, Queen's University Belfast, Medical Biology Centre, 97 Lisburn Road, Belfast BT9 7BL, Northern Ireland, UK.
E-mail address: r.donnelly@qub.ac.uk (R.F. Donnelly).

https://doi.org/10.1016/j.bioadv.2022.213073
Received 12 June 2022; Received in revised form 23 July 2022; Accepted 3 August 2022
Available online 9 August 2022

post-surgery [7].

One of the drugs that is frequently used in the treatment of skin and soft tissue infection caused by *B. fragilis* is metronidazole (MTZ). The drug is a nitroimidazole derivate which exerts its antimicrobial effect through the reduction of the nitro group on the drug by the bacterium which leads to the formation of toxic metabolites. Such metabolites exert their bactericidal activity *via* molecular DNA destabilisation, as well as inhibiting DNA repair mechanisms, thus further exacerbating the DNA damage imposed [8]. The DNA damage imposed by the nitroimidazole metabolite ultimately results in bacterial cell death. The drug is typically applied to the skin either as a gels, lotions or cream for the management of superficial infection such as erysipelas. However, for more deep-rooted skin infections, such as cellulitis, the drug is administered *via* the oral route as tablets or *via* intravenous infusion [9]. Although delivering antibiotic *via* the oral route may prove to be convenient, the oral administration of MTZ is associated with gastrointestinal side effect such nausea and vomiting, in addition to the bitter metallic aftertaste [10]. In addition, the enteral delivery of MTZ poses the potential risk of inducing dysbiosis within the gut microbiome. This may give rise to rapid enrichment of antimicrobial resistance genes (ARGs), which can be passed on within the faeces, thus further promoting the antibiotic resistance to other environments [11]. On the other hand, intravenous administration of MTZ may prove to be both invasive and painful which may not be ideal for patients especially those with needle phobia. Indeed, there is a need to reformulate MTZ using an alternative drug delivery strategy which offers a more targeted delivery of the antibiotic for the treatment of SSTIs in a minimally invasive manner.

One pharmaceutical strategy that could be investigated to improve the delivery of MTZ into the skin for the treatment of SSTI are microneedles which are also known as microarray patches (MAPs). Unlike the conventional transdermal patch which is reliant on passive diffusion of actives into the skin, MAPs circumvent the protective barrier of the *stratum corneum* by physically piercing this outermost layer of the skin with microprojections. The application of MAPs to the skin will then result in the formation of water-filled channels within the skin strata which can then be exploited for the delivery of therapeutics such MTZ into the skin [12]. Recent studies have shown that reformulating antibiotics such as MTZ into nanocarrier may prove to be a viable strategy to improve the efficacy of the compound due to its solubility properties which slightly soluble in water [13]. For instance, a clinical comparative study by Badawi reformulating MTZ into solid lipid nanocarrier improved the efficacy of the drug relative to commercial benchmark Metron® for the treatment of bacterial vaginosis [14].

It is worth pointing out that the delivery of MTZ *via* the use of nanosuspension (NS) or MAPs has indeed been demonstrated before. For instance, Latha et al. [13] demonstrated that formulating MTZ as magnetite nanosuspension offered enhanced anthelmintic activity against *Pheretima poi* relative to the vehicle and control formulation. The work by Latha and co-workers highlighted the value of reformulating the MTZ into nanocarriers as a means to enhance the antimicrobial effect of the drug. Even though formulating MTZ as NS offered enhanced efficacy, due to the size of the NS coupled with the barrier properties of the *stratum corneum*, the use of NS alone would not suffice to deliver the drug into the deeper layers of the skin strata. On the other hand, Garland et al. [15] demonstrated for the first time that the use of dissolving MAPs fabricated from poly (methyl vinyl ether co maleic acid) (PMVE/MA) offered a viable strategy to deliver MTZ across the skin resulting in an overall delivery efficiency of ≈ 40 %. However, there is no work to date that have attempted to combine both technologies as a means to enhance the overall delivery of MTZ into the skin, which we have attempted in the current work.

The combination of these two technologies may however offer a viable strategy to enhance the overall delivery efficiency of the MTZ into the skin. Therefore, it is postulated that formulating MTZ into nanocarriers such NS that are loaded into dissolving MAPs may prove to be a viable strategy to deliver the antibiotic into the skin for SSTIs. In the current work, we present the development, characterisation of MTZ-NSs loaded dissolving MAPs as a composite pharmaceutical system for the delivery of the antibiotic into the skin. First, MTZ-NSs were developed *via* wet media milling. The properties of MTZ NSs were investigated and optimised using a composite central design (CCD) software. Upon characterising the NS, the antibiotic was loaded into dissolving MAPs. Upon manufacturing the MAPs, the mechanical and insertion properties of the needles were evaluated in order to understand if the patches were capable of piercing the skin. Following physical and mechanical characterisation of the MAPs, the drug deposition from the formulation across different strata of the skin was also evaluated in order to elucidate the delivery kinetics of the drug from the MAP formulations. This was also complemented with an *in vitro* antibacterial study which was conducted in order to evaluate the effectiveness of the formulation in eradicating cultures of *B. fragilis*. It is hoped that this formulation may serve as a patient-friendly and painless delivery approach of MTZ to treat deep rooted SSTI caused by *B. fragilis*.

2. Materials and methods

2.1. Materials

2-Methyl-5-nitroimidazole-1-ethanol (purity, >99 %) was purchased from Alfa Aesar (Lancashire, UK). Tween® 80 was procured from Tokyo Chemical Industry (Oxford, UK). Soluplus®, Lutrol® F108 and Pluronic® F88 Pastille were kindly supplied by BASF (Ludwigshafen, Germany). PVP 90 kDa was supplied by Ashland (Kidderminster, UK). Ultrapure water used in the work was obtained from Elga PURELAB DV 25 purification system, (Veolia Water Systems, Dublin, Ireland). The remaining materials were of analytical grade and procured from Sigma-Aldrich (Dorset, UK) or Fisher Scientific (Loughborough, UK). *Bacteroides fragilis* NCTC 9343 (National Collection of Type Cultures, Salisbury, UK) was maintained in Brain Heart Infusion (BHI) broth with 15 % glycerol at −80 °C and cultivated in BHI broth at 37 °C for 48 h when required for the microbiological assessments. Full-thickness neonatal porcine skins were obtained from stillborn piglets within 24 h *post-mortem* and stored at −20 °C until use.

2.2. Preparation and optimisation of MTZ-NS

In the present work, the following surfactants- poly(vinyl alcohol) (PVA) 9–10 kDa, Tween®, Pluronic™ F88, Lutrol® F108 and Soluplus® were screened as potential excipients in the preparation of MTZ-NS. The MTZ-NS formulations were optimised in systematic fashion using a design of experiments (DoE) approach. This was achieved using surface responses, composite central design (CCD) with Design Express Software version 11 (State-ease, Minneapolis, USA). In conducting the DoE study for the MTZ-NS, the surfactant and MTZ concentration in tandem with agitation time were used as variables factors to optimise the final formulation. In addition, particle size and PDI were selected as critical outcomes for the DoE study in order to obtain MTZ in homogenous and narrowly distributed particle size [16].

A modified media milling approach was adopted in fabricating the NS, as previously reported [16]. In brief, 0.2 mg of MTZ were added to 12 mL glass vial containing 6 mL of surfactant solution. Four magnetic bars (8 × 4 mm) along with 8 g of zirconia beads (particle size of 0.1 mm) were added to the vial in order to an enclosed micromilling system. Prior to micromilling, the content of the vials was vortexed at 2500 rpm for 30 s. The milling process was instigated by fixing the system to an IKA RCT Basic Magnetic Stirrer (IKA, Staufen, Germany), and agitated at 1500 rpm over the course of 24 h. Upon milling, the NS was separated from the slurry by filtering the mixture through a 200 mesh sieve. The NS was frozen at −80 °C for 3 h prior to lyophilisation for 24 h (Fig. 1).

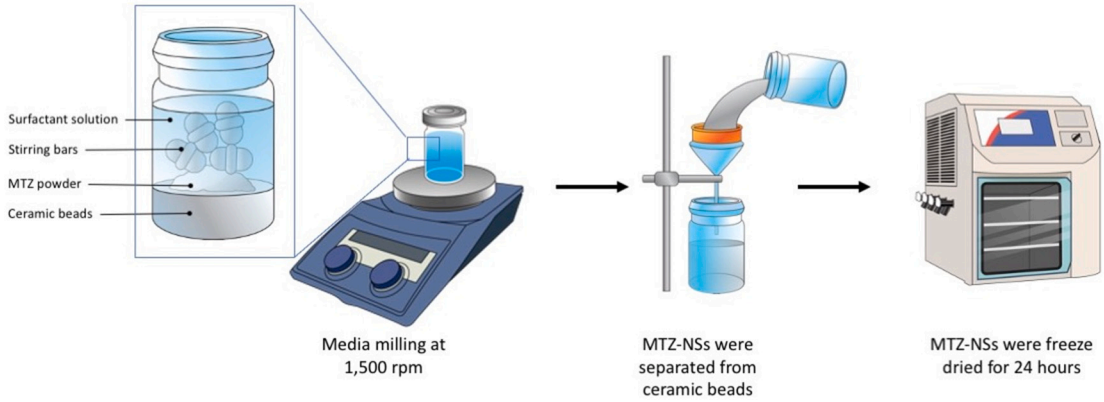

Fig. 1. Schematic representation of MTZ-NS preparation.

2.3. Characterisation of metronidazole nanosuspension

Quasi Elastic Light Scattering was performed on MTZ-NS using a NanoBrook Omni® analyzer (Brookhaven, New York, USA). The NS were evaluated in terms of the size and polydispersity index (PDI) which gives an indicator on the size distribution of the nanoparticles. Prior to sample analysis, the sample was dispersed and diluted (x200 dilution) in an Eppendorf® tube containing 2 mL of distilled water. The NS was then vortexed at 2500 rpm for 60 s before being transferred into a disposable cuvette (length 12 mm, height 45 mm, width 12 mm). Prior to analysis, the sample was subjected to a 3 min equilibration time after which sample analysis was conducted at 25 °C. All measurement made for the NS were done in triplicates, $n = 3$.

Scanning electron microscopy (SEM) TM3030 microscope (Hitachi, Krefeld, Germany) was employed to elucidate the morphology of pure MTZ, pure Soluplus® and PM. The samples were applied onto adhesive carbon tape prior to analysis. Transmission electron microscope (TEM) JEOL JEM 1400-plus transmission electron microscope (JEOL UK, Welwyn Garden City UK) with an accelerating voltage of 120 kV was used to visualise the morphology of MTZ-NS. For TEM analysis, diluted sample was dropped on a copper grid coated with Formvar film and dried at room temperature for 24 h prior to analysis. The chemical interaction between MTZ and surfactant from the optimised formulations was gauged using a Fourier transform infrared (FTIR) spectrometer (Accutrac FT/IR-4100™ Series, Perkin Elmer, USA). The crystallinity of pure MTZ, physical mixture (PM) and optimised MTZ-NS formulations were evaluated using a differential scanning calorimeter, DSC Q100 (TA Instruments, Elstree, Hertfordshire, UK) in tandem with XRPD, X-ray diffractometer (Rigaku Corporation, Kent, England).

2.4. In vitro release study of MTZ-NS

In order to understand the release profile of MTZ from the optimised NS, a side-by-side diffusion cell (Permergear, Hellertown PA, USA) diffusion study was conducted across the SnakeSkin™, 7000 MWCO dialysis membrane (Thermo Fisher Scientific, Altrincham, UK) [17,18] (Fig. 2). The membranes were initially trimmed into 15 mm × 15 mm film and secured to the donor compartment using cyanoacrylate glue. The dialysis membrane was clamped between the donor and receptor compartment followed by the addition of 3 ml PBS pH 7.4 into both compartments. Pure MTZ (10 mg) and MTZ-NSs that corresponded to 10 mg MTZ were individually added and dispersed into the donor compartment. The receptor solution was sampled at predetermined time points and replenished with the same volume of fresh PBS. All samples were then analysed using a validated of high-performance liquid chromatography (HPLC) method, as detailed in Section 2.11.

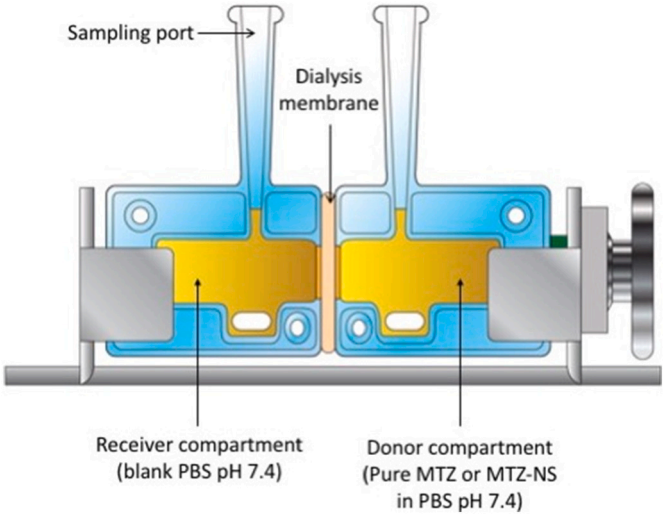

Fig. 2. Side-by-side dialysis setup for *in vitro* release studies of pure MTZ and MTZ-NS.

2.5. Fabrication of dissolving MAPs

Optimised MTZ-NS formulation fabricated from Soluplus® was selected in the manufacture of dissolving MAPs as shown in Fig. 3. In brief, the MTZ-NSs, along with appropriate proportions of deionised water, as detailed in Table 1, was mixed and pipetted (50 mg) into a silicone mould (16 × 16 pyramidal needle density, 850 μm height, 300 μm width at base, 300 μm interspacing and 0.36 cm^2 patch area) to form the needle matrix. The moulds were subjected to a positive pressure of 4 bar for 5 min, followed by the removal of excess of the first layer formulation from the moulds. The needle layers were dried for 30 min under a positive pressure chamber of 4 bars. Flexible elastomer rings (external diameter 23 mm, internal diameter 18 mm, thickness 3 mm) were secured on top of the silicone moulds using a thin layer of aqueous 40 % of w/w PVA (9–10 kDa). Upon drying the moulds under ambient condition for 6 h, 850 μL of an aqueous blend of 30 % w/w of PVP (90 kDa) and 1.5 % w/w of glycerol was added followed by centrifugation at 3500 rpm for 10 min. Upon drying the moulds at ambient condition for 24 h, excess sidewalls that were formed during manufacture were meticulously removed using a pair of scissors. Finally, the MAPs were transferred and dried at 37 °C for 24 h before the formulations were subjected to characterisation.

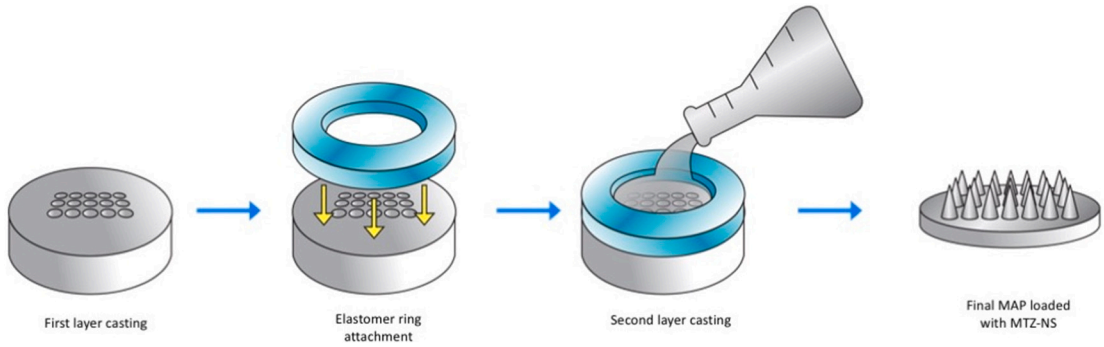

Fig. 3. Schematic representation of fabrication of MTZ-NS loaded dissolving MAPs.

Table 1
Formulations for first layer of dissolving MAP preparation.

MAP formulation code	MTZ-NS powder (%)	Deionised water (%)
F1	50	50
F2	33	67
F3	25	75

2.6. Microneedle compressive resistance and insertion evaluation

The structure of the MAPs was imaged using a digital light microscope (Leica EZ4 D, Leica Microsystems, Milton Keynes, UK). The physical traits and thermal transition of the neat drugs and MAPs formulations were evaluated *via* differential scanning calorimetry (DSC Q20, TA Instruments, Elstree, Hertfordshire, UK). This was performed in order to gauge if formulating the drug into MAPs may result in any changes to the solid state of the drug.

The resistance of the MAPs to a compressive force of 32 N was investigated using a TA-TX2 Texture Analyser (TA) (Stable Microsystems, Haslemere, UK) as previously described [19,20]. A force of 32 N was chosen as the target compressive force as this is normally the force encountered by the patch during skin application. The resistance of the MAPs to the force was evaluated as a change in height of the needles after being compressed. This was calculated using Eq. (1).

$$\textit{Change in needle height}\ (\%) = \frac{\Delta \textit{needle height}}{\textit{original needle height}} \text{x } 100 = \frac{H_a - H_b}{H_a} \times 100\% \quad (1)$$

where H_a is the original needle height and H_b the height of the needle after being compressed for 30s under 32 N.

As one of the cardinal features of MAPs is the ability of the patch to puncture the skin upon application, the insertion profile of the formulations was also investigated. Firstly, the insertion of the MAP into eight stacks of Parafilm® M layer was done in order to gauge the insertion efficiency of the formulation with each layer. Parafilm® M was chosen as a skin simulant in this instance. Complementary to Parafilm® M insertion study, the ability of the MAP to puncture *ex vivo* full thickness neonatal porcine skin was also conducted. When conducting this experiment, EX-101 optical coherence tomography (OCT) microscope (Michelson Diagnostics Ltd., Kent, UK) was used to see the needle insertion into the skin under real-time [21]. The images collected from OCT analysis was then processed and analysed using ImageJ® (National Institutes of Health, Bethesda MD, USA) in order to gauge the length of the needles that have been inserted into the skin [22]. On top of that, OCT was also used to visualise and evaluate how the MAPs dissolve within the skin *in situ* over the course of 60 mins.

2.7. Drug content localised in the needles

MAPs were individually placed in a glass vial containing 4 mL of deionised water and sonicated for 30 min to dissolve them. The mixture was diluted by the addition of 4 mL of acetonitrile and sonicated for a further 30 min. The final drug containing solution was centrifuged at 14,500 rpm for 15 mins prior to HPLC analysis.

2.8. In situ dissolution studies

In order to evaluate the time taken for the needles on the MAPs to dissolve in the skin, an *in situ ex vivo* skin dissolution study was conducted. Briefly, excised full-thickness neonatal porcine skin was immersed in PBS (pH 7.4) for 30 min and allowed to equilibrate to ambient temperature prior to the experiment. MAPs from F1–F3 were inserted to the skin using manual thumb pressure for 30 s. In order to mitigate the propensity of the patch to dislodge from the skin, stainless-steel cylindrical weights (15.0 g) were secured on top of the MAP [23]. The samples were then incubated at 37 °C in a thermostatically controlled oven. At predetermined time, the MAPs were meticulously peeled from the skin and the morphology of MAPs were visualised and captured under a digital microscope.

2.9. Biocompatibility study

MTZ-NS biocompatibility on fibroblast like cells (3T3L1) was evaluated by 3-(4,5-dimethylthiazol-2-yl)-2,5-diphenyl tetrazolium bromide (MTT), LIVE/DEAD™ and cell proliferation assays. Initially, all MAPs were sterilised using UV light at 253 nm for 7 mins. Fibroblast-3T3L1 cells were plated and incubated on MAPs cultured with complete DMEM culture medium (DMEM-F12-GlutaMAX-I, Gibco, New York, NY, USA) for 72 h at 37 °C with 5 % CO_2. MTT assay was conducted as previously described [24]. The culture medium was replaced MTT solution (0.5 mg/mL) in DMEM. After 5 h, the supernatant was removed, DMSO was added (200 μL), and the sample was gently shaken for 15 min to allow the dissolution of the formazan crystals. Optical absorbance was measured using a Synergy H1 microplate reader (Biotek, Winooski, VT, USA) at 570 nm. DMEM F12 medium was used as a negative control, and Triton X-100 (1 %) was used as a positive control. In order to confirm cell viability, live/dead staining was conducted. Firstly, MTZ-NS and Soluplus® samples were added to 3T3L1 cell culture for 72 h. The cells were then stained for 5 min at room temperature in 5 μg/ml calcein AM and 5 μg/ml ethidium homodimer-1 (Molecular probes, Eugene, Oregon). In addition, cell proliferation was also evaluated *via* DNA content assay. The nucleic acid concentration, DNA, from the cells that have adhered to the samples (MTZ-NS and Soluplus®) was assayed using Quant-iT™ PicoGreen® dsDNA Reagent and Kits (Molecular Probes, Life Technologies Corp.). This was done based instructions provided by the kit. In brief, the cells were meticulously rinsed with PBS (pH 7.4) for a total of three times before being treated with 1 mL of lysis buffer that

consist of 10 mM Tris (pH 8), 1 mM EDTA, and 0.2 % (v/v) Triton X-100. Next the samples were vortexed for 10 s after an interval of 5 min for a total of 30 min. During this step, the cells were kept on ice throughout the entire process. This step was done in order to promote the release of nucleic acid from the cells. Next, the cells were carefully thawed on ice before being homogenised for 10–15 min. 100 μL of DNA-binding fluorescent dye solution was pipetted into the samples to promote the binding of the fluorophore to the DNA that has been release. The fluorescence intensity was measured at an excitation wavelength of 480 nm and an emission wavelength of 520 nm. A standard curve was constructed using Lambda DNA order to quantify the amount of DNA that is being assayed. Sample analysis were done in triplicates ($n = 3$).

2.10. Dermatokinetic study

Dematokinetic studies using a Franz cell (Permergear, Hellertown PA, USA) set up were implemented in order to evaluate the delivery of MTZ from the composite MAP system across the full thickness neonatal porcine skin. Briefly, full thickness *ex vivo* neonatal porcine skin was trimmed and carefully glued to the donor compartment using cyanoacrylate glue. The MAP insertion into the *ex vivo* neonatal porcine skin was performed under manual thumb compression for 30 s. On the other hand, PBS (pH 7.4) which had been warmed to 37 °C and degassed was added to the receiver compartment of the Franz cells. The solution was maintained at 37 ± 1 °C and stirred at 600 rpm. The donor compartment was then attached to the receiver compartment. The MAP was secured in place by the addition of a stainless-steel cylindrical weight (15.0 g) as previously reported, in order to prevent MAP expulsion from the skin [23]. The evaporation of receiver solution was mitigated by sealing the sampling arm using Parafilm® M. At pre-determined intervals, the Franz cells were dissembled, and 1 mL of receiver media and the porcine skin was collected and analysed. The release media was centrifuged at 14,500 rpm for 15 mins and then filtered using 0.45 μm PTFE filter prior to HPLC analysis. The skin samples that were collected at pre-determined time were heated treated at 60 °C using hotplate for 5 mins. This was done to induce the separation of the epidermis and dermis [25]. The separated epidermis samples were placed in an Eppendorf tube contained 2 mL of acetonitrile, homogenised using thermal mixer (ThermoMixer™F2.0, Eppendorf, Hamburg, Germany) for 30 min. In contrast, the separated dermis was placed in an Eppendorf tube contained 0.5 mL deionised water and then homogenised using a Tissue Lyser LT (Qiagen Ltd., Manchester, UK) at 50 Hz for 15 min to dissolve the hydrophilic polymer. Next, 1 mL acetonitrile was added to the Eppendorf tube followed by a further homogenisation step for 15 min. Lastly, all samples were centrifuged at 14,000 rpm for 15 mins followed by the injection of the supernatant into the HPLC column. Where necessary, samples and external standards were diluted in PBS (pH 7.4).

2.11. In vitro antibacterial activity of MTZ-NS loaded microneedle arrays

MAPs loaded with MTZ-NS were tested for inhibitory effects on bacterial cultures of *Bacteroides fragilis* NCTC 9343, which is an obligate anaerobic gram-negative bacillus associated with SSTIs [6]. For this purpose, *B. fragilis* was incubated under anaerobic conditions on BHI broth at 37 °C for 48 h. Subsequently, the inoculum (20 mL) was centrifuged at 3500 rpm for 15 min and the pellet was re-suspended in 5 mL of the same broth in order to concentrate it. Then, 100 μL of this concentrated inoculum was poured and plated on the BHI agar plate by using a cotton swap in order to obtain a bacterial lawn. After that, the plates were allowed to dry for 15 min and the MAPs were then placed on the top of the BHI agar plates and incubated under anaerobic conditions at 37 °C for 48 h. Further, inoculated plates with *B. fragilis* alone and containing MAPs with no MTZ-NS were also incubated as positive and negative controls, respectively ($n = \geq 4$).

2.12. High performance liquid chromatography analysis

The concentrations of MTZ were measured *via* HPLC (Agilent Technologies 1220 Infinity UK Ltd., Stockport, UK). HPLC analysis was done using Phenomenex® Luna C18 (ODS1) column (150 mm × 4.6 mm i.d. with 5 μm particle size). A flow rate of 1 mL/min was chosen for sample analysis and this was done at 25 °C. The mobile phase consisted of methanol as the organic phase while the aqueous phase consisted of water with 0.1 % triethylamine (40:60 v/v) adjusted to a of pH 6.8. Sample detection was conducted at a wavelength, λ of 322 nm. The injection volume of the sample was 20 μl. The HPLC assay used in the current work has been validated as per International Council on Harmonisation (ICH) 2005 guideline.

2.13. Statistical analysis

Data collection and interpretation was conducted using GraphPad Prism® version 8.0 (GraphPad Software, San Diego, California, USA). The data presented in the current work are displayed as means ± standard deviation (SD), unless stated otherwise. When two treatment groups are compared, a Student's *t*-test was done. In contrast, when the analysis entails the comparison of multiple groups, One-way analysis of variance (ANOVA) was opted instead. Statistical significance was deemed at $p < 0.05$. Besides that, additional level of statistical significances was denoted using the following convention 0.033(*), 0.002(**), <0.001(***) and < 0.0001 (****).

3. Results and discussion

In the current work, we developed a composite pharmaceutical system consisting of MAPs loaded with MTZ-NS in an attempt to improve the treatment of localised skin infections caused by *Bacteroides fragilis* spp. This composite pharmaceutical system utilises a NS strategy to reduce the particle size and convert MTZ into an amorphous state which would improve the solubility and thus the drug loading of the antibiotic into the patch. In addition, this formulation also capitalises on the penetration capability conferred by MAPs to improve the intradermal deposition of the antibiotic.

3.1. Preparation of MTZ-NS

In order to develop this composite formulation system, a series of surfactants were first screened in the development of MTZ-NS in order to identify which surfactant would be capable of forming a NS with the smallest particle size (nm) and narrow size distribution (PDI).

During the preliminary screening study, a surfactant concentration of 2 % w/w was selected. This concentration was selected based on previous study which showed that this concentration was sufficient to produced NS with small particle size and low PDI [16]. Fig. 4 shows the particle size and PDI of MTZ-NS when the drug was nano-milled with different surfactants over the course of 24 h.

It is apparent that without the addition of surfactant (control), the nano-milling process resulted in MTZ with a particle size of ≈200 nm. During the milling procedure, the formation of NS is a result of two competing processes that are occurring simultaneously: particle breakage and aggregation [26]. Particle attrition that contributes to MTZ size reduction is attributed to the physical and mechanical grinding between the drug particle with the milling media, in this case the zirconia beads. In contrast, upon undergoing particle size reduction, the resulting drug particles have a tendency to aggregate due to inherent attractive forces arising from inter-particle forces such as van der Waals and even hydrophobic-hydrophilic attraction [27]. Therefore, in order to mitigate the particle aggregation, the manufacture of NSs typically includes the addition of polymeric stabilizers or surfactants during the milling step. The surfactant stabilizes the newly formed nanosized drug particles' surfaces, which mitigates particle aggregation post-

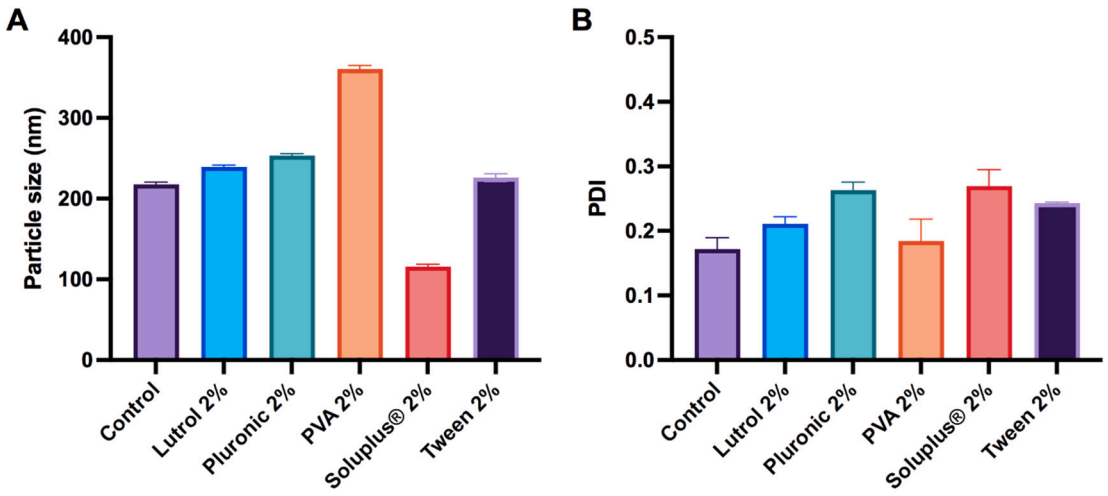

Fig. 4. Metronidazole nanosuspension (MTZ-NS) characterisation. The NSs were fabricated using different surfactants (2 % w/v) *via* nanomilling. (A) particle size and (B) PDI. Data presented as mean + SD ($n = 3$).

manufacture. It can be seen that the addition of Tween, Lutrol and Pluronic resulted in drug particle sizes roughly the same size as the control. In contrast, we observed that the use of PVA resulted in a NS displaying the highest drug particle size. We also observed that the use of Soluplus®, a grafted copolymeric solubilizer, resulted in MTZ-NS with the smallest drug particle size, ≈100 nm. Such enhanced drug particle size reduction in this instance may be attributed to the combination of physical attrition of drug particle size due to media-milling along with the enhancement in drug solubilizing effect of the Soluplus® [28]. In the current work, we observed that the choice of surfactant used in the manufacture of NS plays a critical role in determining drug particle size. Such a finding echoes with the findings of other researches, who have shown that the choice of stabiliser plays a critical role in the overall particle size of the NS [29–31]. In the current work, we have screened and chosen the surfactant that resulted in the formation of MTZ NS with the smallest particle size. This is based on the findings from several publications to date that have shown that the size of the nanocarriers has an impact on the overall antimicrobial properties of the formulation, with smaller nanoparticles conferring the greatest bacteriostatic and bactericidal activities. For instance, Dong et al. [32] have demonstrated that the use silver nanoparticles with a size of 10 nm conferred superior bactericidal activity relative to larger nanoparticles used in their work. This work echoed the earlier work by Inam et al. [33] who demonstrated that methyl-quaternized nanoparticles displaying a size of less than <1 μm exhibited enhanced antibacterial activity against seven different strains of bacteria relative to the larger methyl-quaternized nanoparticles. Upon identifying the surfactant which offers the smallest particle size and the lowest PDI during media-milling, a design of experiment (DoE) study was conducted in order to optimise the NS formulation.

The optimisation of NSs was carried out using CCD which entailed the use of 15 formulations that were suggested by the software. Particle size and PDI were recorded before and after freeze drying as the responses for all NS formulations, presented in Table S2 and Table S3. The representative 3D surface graphs describing the effect of parameter on the particle size and PDI before and after freeze drying are presented in Fig. 5. The optimum formulation was selected based on the highest desirability factor for minimum particle size and PDI, as generated by the software. This is presented in Table 2 as the predicted and observed values of particle size and PDI for the optimised NS formulation. The optimised formulation consisted of 10 % w/v Soluplus® solution, 800 mg MTZ that was nano-milled with an agitation time of 30 min. As bias value of optimised formulations in all cases were <15 %, this indicated that the optimisation process of NS formulation was indeed successful [34,35].

3.2. Characterisation of MTZ-NS

Fig. 6A-C show the SEM images of pure MTZ, pure Soluplus® and PM, respectively. Fig. 6D displays the TEM image of MTZ-NS. The size of NC in this experiment was found to be <100 μm, which is similar to that observed in DLS analysis. Fig. 6E shows the FTIR spectra of pure MTZ, pure Soluplus®, PM and MTZ-NS. All the characteristic peaks in pure MTZ spectra were also found in the PM and NS formulation, indicating no interaction between MTZ and Soluplus®. Furthermore, XRD and DSC thermal analysis were performed to evaluate the crystallinity state of MTZ during the milling process, which are shown in Fig. 6F and Fig. 6G, respectively. The diffractogram of pure MTZ displayed several sharp peaks at the following diffraction angles (2θ) of 12.94°, 19.24°, 25.29°, and 29.46°, which indicates that MTZ is present in a crystalline form. These characteristic peaks were also observed in the PM but were absent in the MTZ-NS, which shows suggest the drug was in an amorphous state. Moreover, DSC thermal analysis was performed to verify the XRD results. All endothermic peaks remained sharp at 162 °C, representing melting point and crystallinity of MTZ in the diffractograms of pure drug and PM. However, this peak was not found in the MTZ-NS thermogram, confirming that the optimised NS formulation is presented as amorphous structure [36–38]. These results suggest that wet-bead milling technique used to prepare MTZ-NS also resulted in the amorphization of the drug. These results are consistent with previous findings for other drugs such as dexamethasone and tacrolimus [39]. It has been reported that mechanical pressure during the milling process generates lattice vibrations contributing to the amorphisation of the sample [40]. However, it is important to note that amorphization does not always happen during wet-bead milling as in multiple cases the resulting NSs obtained using this technique still remain crystalline [41,42]. The formation of amorphous NSs is linked to the properties of the drug/stabiliser and the process parameters [40].

3.3. In vitro release study

In vitro release profiles of pure MTZ and MTZ-NS formulation are presented in Fig. 6H. The results show that, by formulating the drug into an NS formulation, the release percentage of MTZ was significantly enhanced ($p < 0.0003$) up to 72 % over 24 h. Conversely, the drug released from pure MTZ was only 11 % after 24 h. In addition, we also observed that when the release study was done using pure MTZ in the presence of Soluplus® as a physical mixture (PM), the release profile

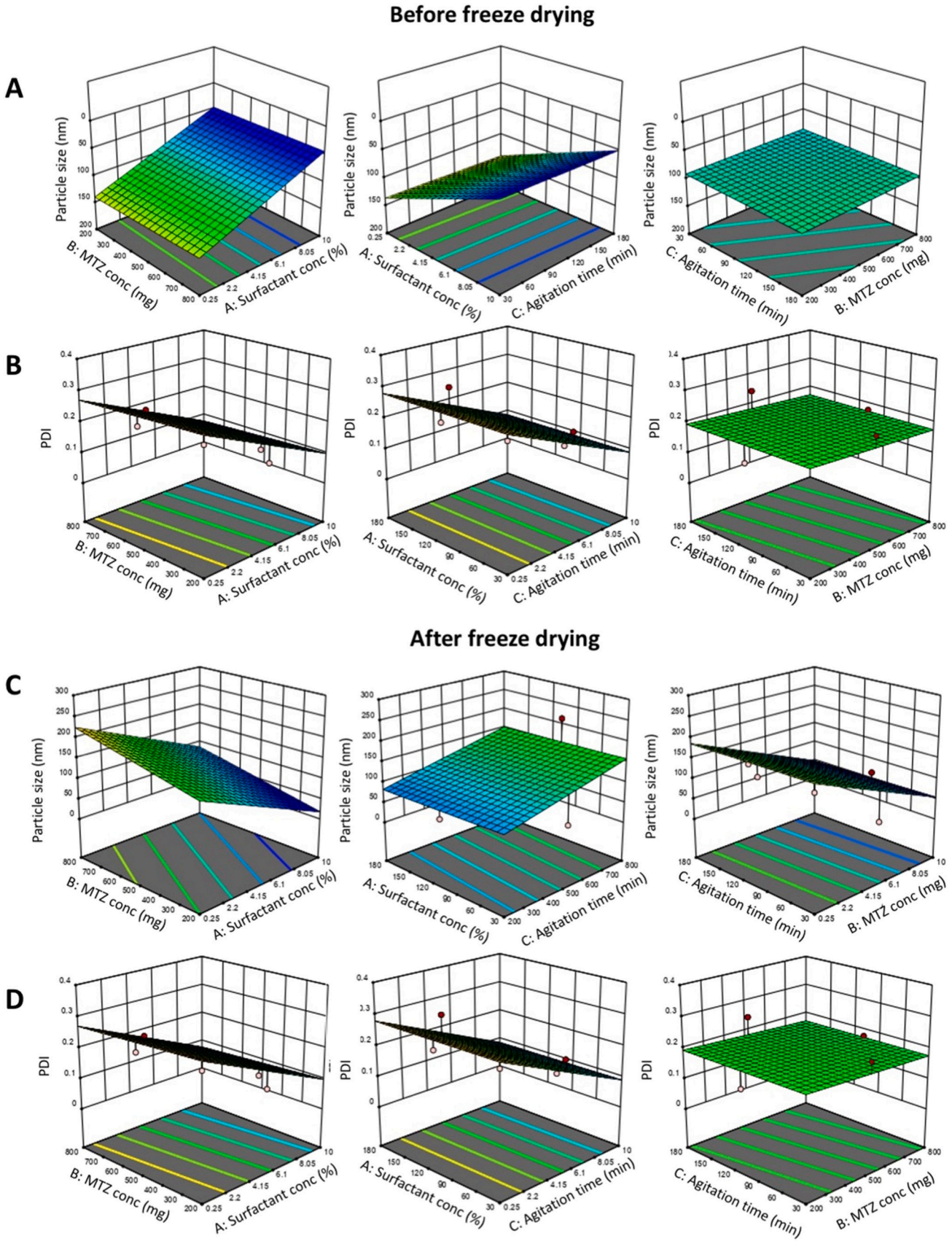

Fig. 5. Response surface plots describing the effect of surfactant concentration, MTZ amount and agitation time to the (A,C) particle size and (B,D) PDI of MTZ-NS formulation prior and post freeze drying process.

Table 2
Predicted and observed responses of the optimised MTZ-NS formulation.

	Factors			Responses	Predicted	Observed (mean ± SD, $n = 6$)	Bias (%)
	Surfactant concentration (% w/v)	MTZ concentration (mg)	Agitation time (min)				
Before FD	10	800	30	Particle size (nm)	42.26	46.70 ± 3.32	−10.5
				PDI	0.09	0.09 ± 0.01	6.12
After FD	10	800	30	Particle size (nm)	89.21	79.35 ± 3.87	11.06
				PDI	0.08	0.08 ± 0.01	2.74

obtained was similar to that of pure MTZ. This suggest that the presence of Soluplus® alone was insufficient to promote the release profile of unmodified MTZ but necessitate the reformulation of the pure drug into NS in order to achieve a more rapid and greater release profile. This is possibly due to the larger surface area of NS formulation, which leads to an increase in the dissolution rate and solubility [16,36,43]. In addition, the presence of poly(ethylene glycol) (PEG) on the structure of Soluplus® endow the polymer with enhanced hydrophilicity. Thus, incorporating this polymer in the fabrication of MTZ nanoparticles will lead to formation of nanosuspension with enhanced hydrophilicity. This in tandem with the overall reduction in drug particle size will ultimately lead to a significant increase in the rate of drug dissolution thus promoting the solubility and release of MTZ.

3.4. Mechanical resistance, drug content and ex vivo skin insertion study

Upon optimising the MTZ-NS, the formulation was then used to fabricated dissolving MAPs. The resulting MTZ-NS loaded dissolving polymeric MAPs are shown in Fig. 7. For all three MAP formulations evaluated, the digital microscope images revealed sharp obelisk needles on a clean and smooth baseplate when the MTZ-NS were casted and dried. The F1 MAPs manufactured from MTZ-NS appeared clear and transparent, while those with higher percentages of MTZ-NS appeared off-white in the tip of the needles, as shown in Fig. 7.

It is also worth noting, we have attempted to fabricated MAPs using pure MTZ which has not been formulated into NS, however, this formulation had poor needle fidelity post-fabrication as shown in Fig. S1 and was not viable to be used as a control formulation in the current work.

Following visual inspection of the MAPs, a series of characterisation experiment were conducted in order to evaluate the mechanical properties and insertion capabilities of the needles. It can be seen from Fig. 8A that the dissolving MAPs fabricated displayed similar percentage height reduction of 4–5 % when the MAPs were subjected to a compressive force of 32 N [44]. It can also be seen from Fig. 8A, when the fabricated MAP was void of any drug, the overall formulation had a lower mechanical resistance against a compressive force of 32 N. This caused the blank MAP to experience an overall greater height reduction of ≈16 % relative to the drug loaded formulations. In this instance, drug loading did impact the mechanical properties of the formulation by enhancing the resistance the MAPs against compression. It is postulated that in this instance, the presence of MTZ within the MAP function as an external plasticiser which endowed the needles with greater resistance against mechanical compression. Such finding is corroborated by the findings of Siepmann et al. [45] that demonstrated the role of drug molecules as an external plasticiser within polymeric systems. It was apparent that, in this instance, the drug loading of MTZ-NS in the MAPs did not affect the overall mechanical properties of the needles. This resulted in the formation needles which displayed similar mechanical properties despite having varying drug loading as shown in Fig. 8B. The percentage height reductions observed were similar to the values that have been reported by other researchers in the fabrication of dissolving MAPs [46,47]. This would suggest that the fabricated MAPs would possess sufficient mechanical robustness to withstand the manual pressure during MAP application into the skin. With respect to drug loading, we observed formulation F1 and F2 which had a higher ratio of MTZ-NS powder: deionised water displayed a lower drug loading to F3 which had the lowest MTZ-NS powder: deionised water ratio. Intuitively, it is postulated that MAP fabricated with the highest MTZ-NS powder: deionised water ratio, in this case F1, would exhibit the highest drug loading. Nevertheless, this was not the case as we observed formulations F1 and F2 which were fabricated at a higher percentage of MTZ-NS powder, resulted in expulsion of NS aqueous blend out of the mould, which were later removed *via* scrapping, after the formulation has been subjected to a positive pressure of 4 bar for 5 min. In contrast, this was not observed when F3 was fabricated at a lower percentage of MTZ-NS powder, resulting in higher drug loading into the needle layer.

Next, an insertion study of the MAPs into a skin simulant consisting of eight layers of Parafilm® M was conducted in order to investigate the insertion profile of the MAPs. It can be seen from Fig. 8C that all three MAP formulations displayed similar insertion profiles, capable of being inserted all the way down into the third Parafilm® M layer. For all three formulations evaluated, we observed that all of the MAP formulations fabricated were capable of puncturing the first layer of Parafilm with 100 % insertion efficiency in a consistent fashion, as evinced by the absence of any error bars in the first layer. Next, an insertion study utilising full thickness *ex vivo* neonatal porcine skin was conducted in order to evaluate further the insertion performance of the MAPs fabricated. OCT was implemented to visualise the insertion of needles *in situ* into the skin, as shown in Fig. 8D. It can be seen that all three formulations resulted in similar skin insertion depths of ≈ 600 μm, despite having varying drug loadings. Pathogenic bacteria which typically result in skin infection have been shown to be present not only on the surface of the skin but, in some instances, reside deep within the epidermis and dermis [48]. Therefore, all three MAPs loaded with MTZ-NS were shown to puncture the skin, resulting in intradermal deposition of drug loaded needles to a depth of 600 μm. This insertion depth was into the 400–700 μm which is frequently cited as the region in which pathogenic bacteria typically reside during skin infection [49].

This is the first report that describes the use of MTZ-NS combined with MAPs. There are multiple examples of NSs loaded into MAPs described in the literature [41,50–54]. The MAPs described here have shown similar behaviour to those previously reported with respect to insertion and mechanical properties. Tekko et al. [51] prepared MAPs loaded with methotrexate nanocrystals showing equivalent insertion profiles and height reductions after compression (lower than 10 % original needle height) than the ones reported here [51]. It is important to note that the MAP systems prepared by Tekko et al. were similar in terms of needle length and needle spacing. Moreover, McCrudden et al. [52] prepared MAPs loaded with a commercial rilpivirine NS showed similar insertion profiles than the ones described here. In this case the patches contained a slightly lower needle density (14 × 14) than the ones described in the current work (16 × 16). On the other hand, Abdelghany et al. [54]prepared microneedles loaded with curcumin NSs. The resulting MAPs showed a better insertion capability than the ones described here. However, these curcumin-loaded MAPs was fabricated with a lower needle density (11 × 11 *vs.* 16 × 16) which enabled higher insertions but decrease the amount of drug loaded into the needles per mm^2. Recently a different needle tip geometry, cuboidal base with pyramidal tip, has been used for the delivery of NSs. These needles can be inserted to deeper layers of the skin due to its higher needle height (900 μm). Interestingly, the mechanical properties were similar

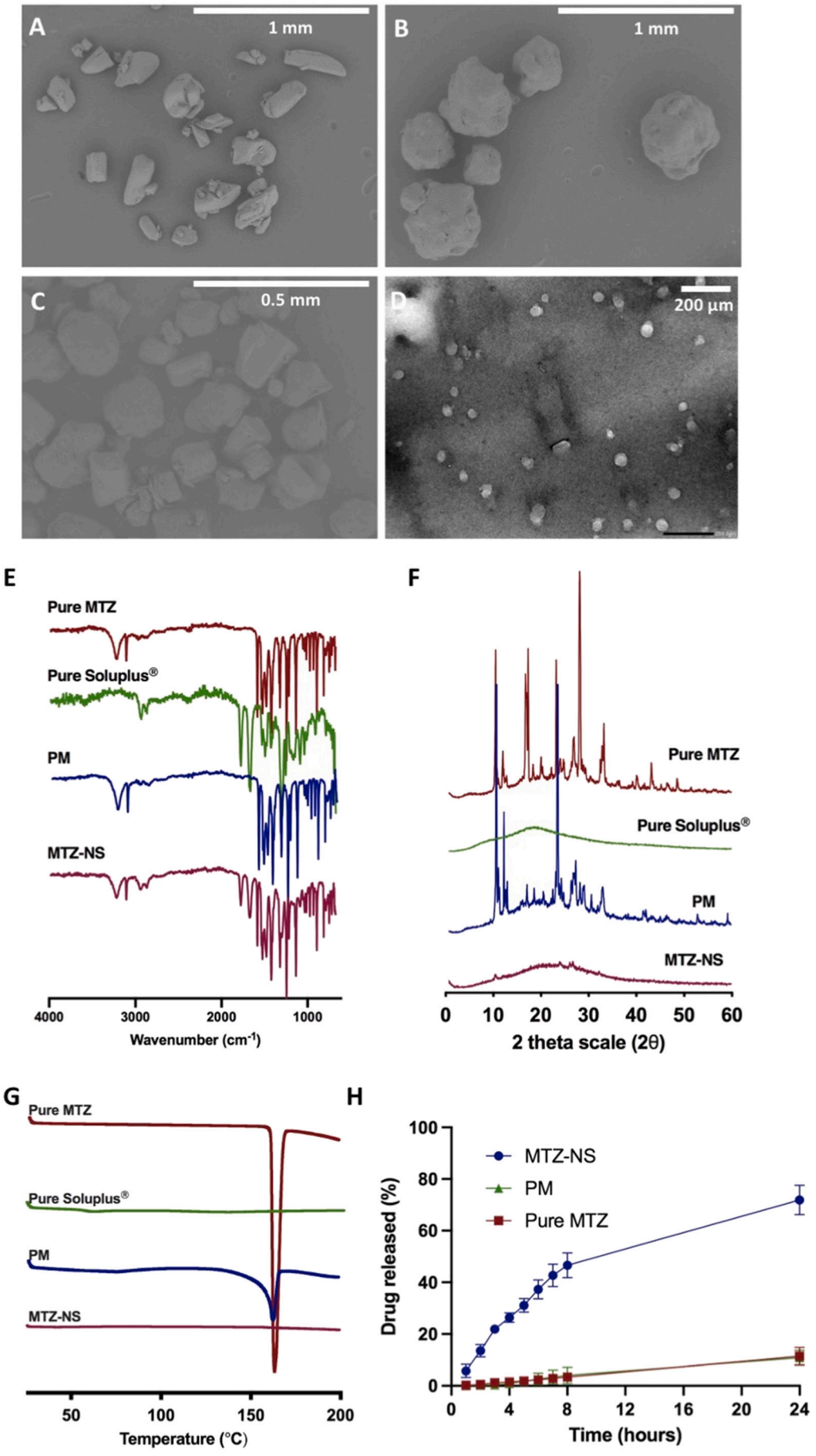

Fig. 6. SEM images of (A) pure MTZ, (B) pure Soluplus® and (C) physical mixture. (D) TEM image of MTZ-NS. (E) Fourier transform infrared analysis of pure MTZ, pure Soluplus®, physical mixture and MTZ-NS. (F) Powder X-ray diffraction of pure MTZ, pure Soluplus®, physical mixture and MTZ-NS. (G) Differential scanning calorimetry thermogram of pure MTZ, pure Soluplus®, physical mixture and MTZ-NS. (H) *In vitro* release profile of pure MTZ, physical mixture and MTZ-NS in PBS (pH 7.4). Data expressed as means ± SD, $n = 3$.

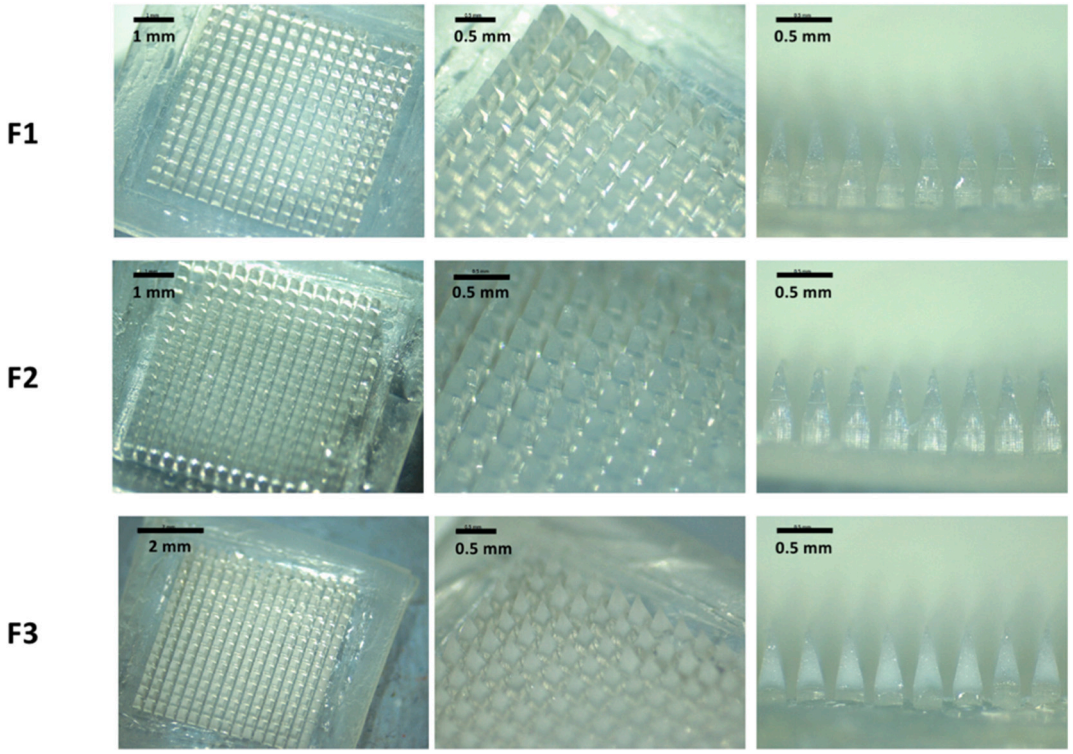

Fig. 7. Digital images of MTZ-NS dissolving MAPs prepared from different ratio of MTZ-NS powder: deionised water.

as the needle height reduction after compression was in line with the one reported in this work [55,56].

Following the *in situ* skin insertion study, we also evaluated the dissolution profile of the needles following patch application to the skin. As shown in Fig. 9, we observed that all three MAP formulations (F1–F3) displayed similar dissolution profile following skin insertion. After 15 min, we observed that a majority of the needle lengths have dissolved and after 30 min we noticed that the whole needle shaft has completely dissolved following skin application for F1–F3. The rapid dissolution profile for all three formulations may be attributed to the hydrophilic nature of the needles which arises due the presence of Soluplus® which function a surface active polymeric solubiliser to accelerate the dissolution of MTZ when the needles are in contact with dermal interstitial fluid [57].

In the current work it can be seen that we have successfully formulated dissolving MAPs which has been loaded with an optimised NS of MTZ. These formulations have been shown to display acceptable mechanical properties enabling effective skin penetration as evinced from the Parafilm® M and *ex vivo* skin insertion study. In order to develop a MAP-based formulation for the management of SSTI, we have chosen the dissolving MAP approach relative to other variants of MAPs. With a dissolving MAP approach, we can easily administer the antibiotic in single-step application process. This is a significant advantage over solid microneedles which necessitate a two-step application process, MAP insertion followed by the topical application of a separate formulation containing the antibiotic. Not only does this introduce an additional step in administering the antibiotic which may cumbersome for patients but the duration by which the pores generated by solid MAPs can vary considerably which may lead dose inconsistencies [58,59]. Such inconsistency in dosing poses the risk of delivering sub-inhibitory concentrations of the antibiotic which may introduce an unwanted selective evolutionary pressure on the targeted bacteria that may ultimately give rise to antibiotic resistance. On the other hand, the use of dissolving MAPs overcome the issue associated with sharp waste post application as this MAP system is inherently self-disabling post application due to needle dissolution within the skin [60]. This is another prominent advantage of using dissolving MAPs over solid and hollow MAPs in order to deliver the NS. Alternatively, one might consider using hydrogel forming MAPs as another strategy to deliver the antibiotic as these variants of MAPs have been demonstrated to deliver high doses of antibiotic transdermally [61]. Although this approach offers the possibility of delivering high doses of antibiotics, recent work has shown that this MAP strategy may in some circumstances result in low drug delivery efficiency due to the drug being trapped in the hydrogel network [34,62,63]. Therefore, due to the disadvantages observed by the other MAPs system, we have decided that a dissolving MAP approach would offer an elegant strategy to deliver MTZ intradermally to treat *B. fragilis* infection.

3.5. Biocompatibility study

It can be seen from Fig. 10A that we observed no reduction in viability when the cells were exposed to MAPs that were either fabricated from Soluplus® alone (blank) or with MTZ-NS. This indicates that that the formulation does not exhibit any noticeable toxicity when tested using fibroblast dermal cell line. This observation are consistent with the findings by Alopaeus et al. [64] and Patnaik et al. [57] showing that Soluplus® did not result in any noticeable reduction in cell viability for HT29-MTX (goblet) and Caco-2 (epithelial) cell lines. Moreover, a PicoGreen assay was also conducted to elucidate the impact of the exposure to the formulation on the proliferation of healthy cells for a 72-hour period. It can be seen in Fig. 10B that exposure of the cells to Soluplus® did not affect the overall proliferation of the cells. On the other hand, exposure of the fibroblast cells to MTZ-NS resulted in a significant enhancement ($p < 0.05$) in cell proliferation. This result can be due to a direct effect of MTZ. Previous reports have confirmed that this drug promotes the proliferation of fibroblasts [65] and could help wound healing [66]. Additionally, these results agree with the results

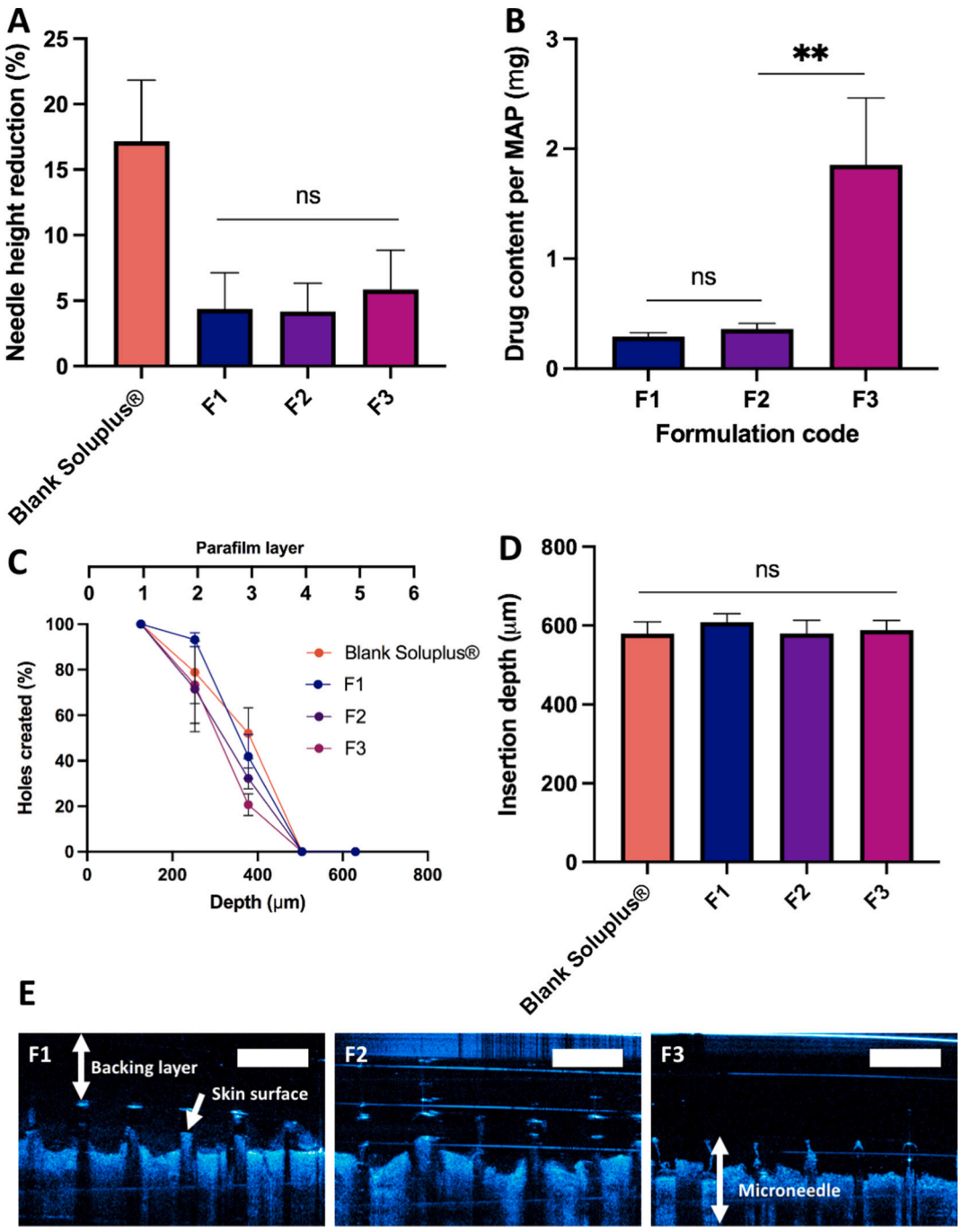

Fig. 8. **(A)** MAP height reduction for needles loaded with metronidazole nanosuspension (MTZ-NS) following application of a force of 32 N (means + SD, $n = 25$). **(B)** Drug content for respective MAP formulations (means + SD, $n = 3$). **(C)** % of holes generated per Parafilm® M layer upon the insertion of MTZ-NS loaded dissolving MAPs (means ± SD., n = 3). **(D)** Insertion depth of MAPs into *ex vivo* skin as quantified from OCT images (means + SD., $n = 20$). **(E)** Insertion of MTZ-NS loaded dissolving MAPs into *ex vivo* neonatal porcine skin monitored using optical coherence tomography (OCT). Scale bar: 500 μm.

reported by El-Shanshory et al. which demonstrated that MTZ significantly boost secondary intention wound healing when administered as nanofibrous scaffolds. The mechanism of action is thought to be related with the ability of MTZ to accelerate wound healing through modulating tissue angiogenesis and collagen production in second intention wounds [67]. On the other hand, the absence of any red fluorescence in Fig. 10C following Calcein/Ethidium Homodimer-1 staining indicated the absence of extracellular nucleic acid released from dead cells with damaged plasma membranes. The observation from Fig. 10C along with the results from Fig. 10A and Fig. 10B probes that the exposure of the cells to the formulation and the polymer did not compromise the viability or plasma membrane integrity of the cells. From a clinical standpoint, the data suggest that delivering MTZ-NS *via* MAP may not result in noticeable toxicity to the skin. In contrast, the ability of the MTZ-NS to promote cell proliferation may contribute to wound healing at the site of infection while the delivery of MTZ would simultaneously stop bacterial infection.

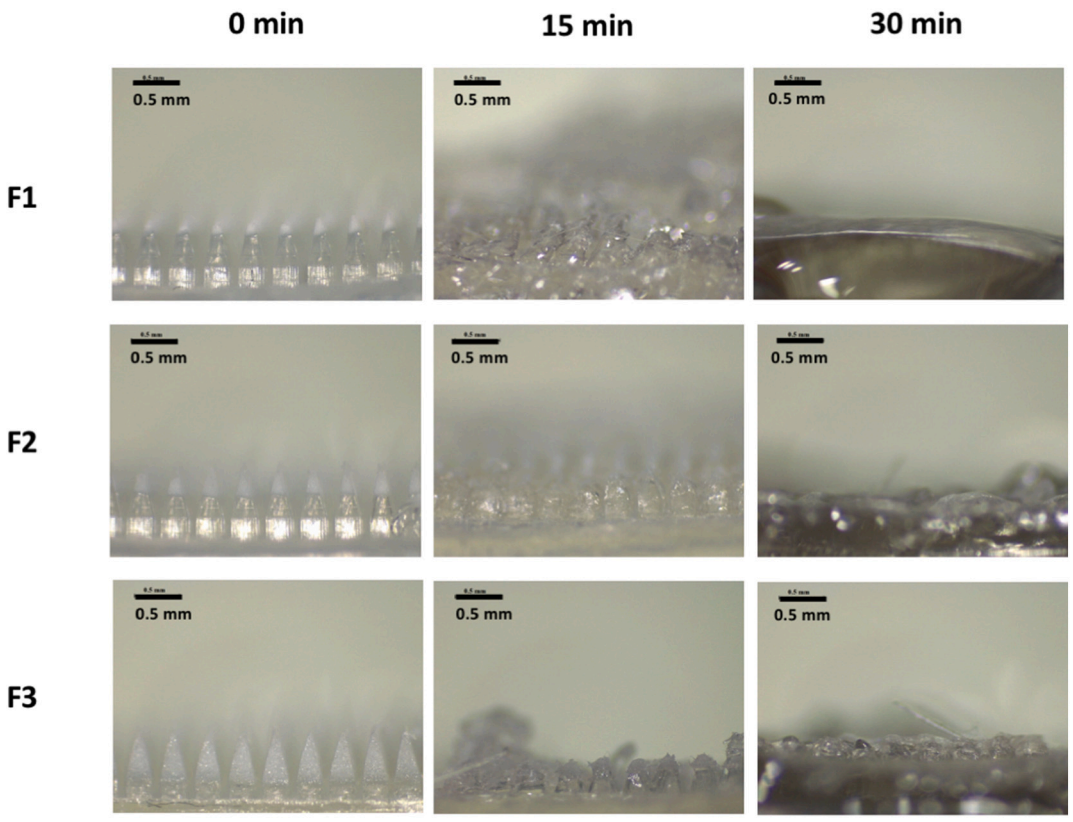

Fig. 9. Digital images of the dissolution of MAPs loaded with metronidazole nanosuspension (MTZ-NS) in F1, F2 and F3 following 0 min, 15 min and 30 min skin application.

3.6. Dermatokinetic study

Following the MAP characterisation and biocompatibility study, F3 was selected for the dermatokinetic study as this formulation offered the highest drug loading while exhibiting similar mechanical and insertion profile relative to the other two formulations. During the dermatokinetic study, a MTZ-NS loaded film which was free-needle patch as control arm. It can be seen from Fig. 11 that the total MTZ that was delivered into and across the full thickness *ex vivo* neonatal porcine skin increased significantly over time from 1 h to 24 h for the MAP treatment arm. In contrast, when the skin was treated with the MTZ-NS film, we observed no delivery of the antibiotic either into or across the skin. Nevertheless, it can clearly be seen from Fig. 11, that MTZ-NS was loaded into MAPs resulted in significant intradermal and transdermal delivery of the antibiotic. This may be attributed to the ability of the MAP to puncture the lipophilic *stratum corneum*, resulting in the intradermal deposition of the drug loaded needles into the skin. This would enable needle dissolution that culminated in drug release into the skin [68].

With regards to amounts of MTZ delivered into the different skin strata, we observed that generally there was an increase in the amount of MTZ deposited within the epidermis and dermis layers, as shown in Fig. 11A and Fig. 11B from 1-hour to the 12-hour time point before the amount delivered plateaued. The highest amount of MTZ delivered into the epidermis and dermis was approximately, 100 μg and 50 μg respectively, and such deposition was achieved at approximately the 12-hour time point. In contrast, we observed that the amount of MTZ delivered into the receptor compartment continued to increase over the course of the skin deposition experiment as shown in Fig. 11C, resulting in 1.5 mg transdermal delivery of the antibiotic. This observation may be attributed to the properties of MTZ-NSs, which upon reaching the aqueous rich dermis would enable the drug traverse *via* diffusion across the skin tissue and into the receiver compartment over time [69].

When the amount of MTZ delivered was viewed from as delivery efficiency (%), it can be seen the MTZ-NS loaded MAPs resulted in an increase in delivery efficiency with application time, reaching a 95 % delivery efficiency after 24 h, as presented in Fig. 11D. It should be noted that when the MTZ-NS is formulated as film, which serves as a control relative to the MAP formulation, we observed no permeation of MTZ into and across the skin as evidenced from the absence of any delivery efficiency (0 %) for the film group in Fig. 11D. This shows that formulating the drug as a NS alone was not sufficient to promote the permeation of MTZ into and across the skin. In addition, this also showed the need to formulate the film into microneedle structure which would enable the formulation to breach the *stratum corneum* to enable effective deposition and delivery of the payload into the skin.

In a previous study, Donnelly et al. [20] have investigated the utility of using hydrogel forming MAP in tandem with drug loaded adhesive patch. In their work, Donnelly and co-workers have shown that without the application of any microneedles, the researchers were only able to deliver 75 μg of MTZ across the skin, which amounts to 1.8 % delivery efficiency. However, the combination of drug loaded patch (4.2 mg) in combination of hydrogel forming MAP, fabricated from PMVE/MA crosslinked with PEG 10,000, resulted in enhanced transdermal delivery efficiency of MTZ across the skin by up to 30 % [20]. By comparing the finding of this previous study with our current work, we observed that reformulating MTZ into dissolving MAPs may be viable strategy to

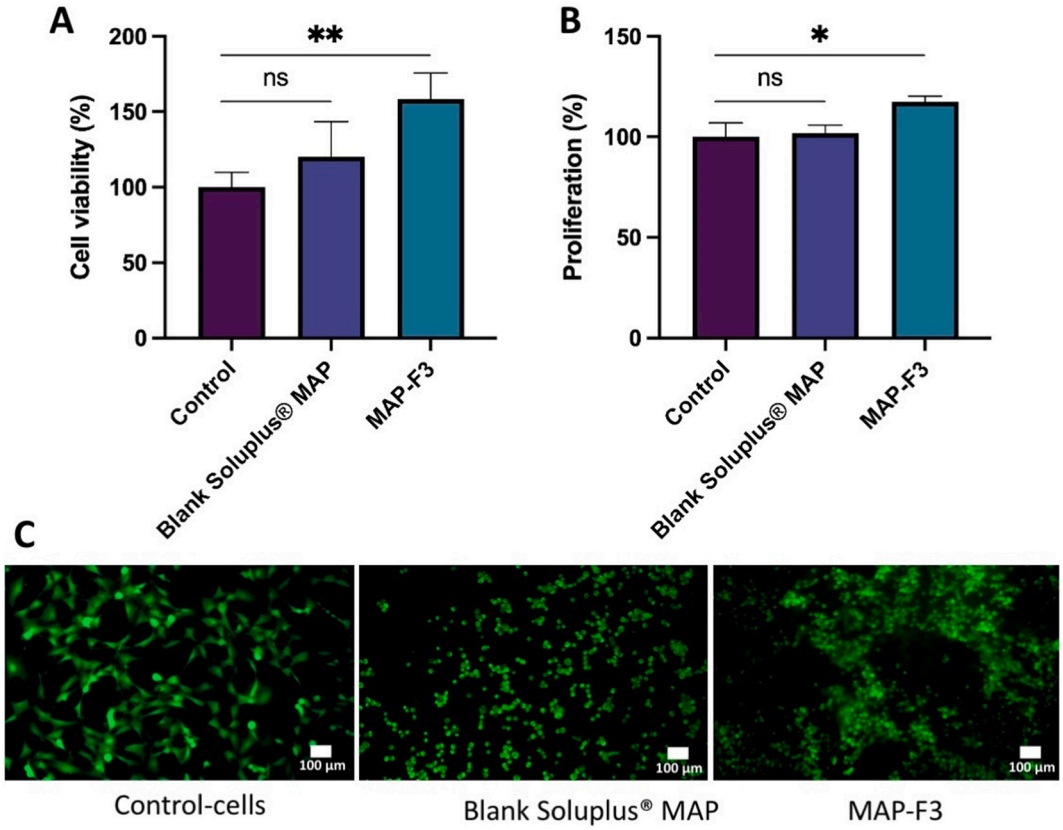

Fig. 10. (A) MTT assay results show the percentage of viable cells after a culture period of 72 h. Fibroblast dermal cells cell viability and proliferation following treatment with MAPs that contained either MTZ-NS or Soluplus®. (B) PicoGreen assay results showing total DNA content of cells on control/coverslip, blank Soluplus® MAPs and MTZ-NS loaded MAPs cultured for a time period of 72 h. A standard curve of known dsDNA (ng/mL) was used to calculate the DNA content from the samples. "**" denotes a statistically significant difference ($p < 0.05$) in cell number with respect to control (plate cells culture). Data points represent means + SD ($n = 3$). (C) Live/dead staining of fibroblastic dermal cells on control (plate cells culture), Soluplus® and MTZ-NS samples. (Green = FDA (live); red = PI (dead)); scale bar = 100 µm. (For interpretation of the references to color in this figure legend, the reader is referred to the web version of this article.)

improve the delivery of MTZ into the skin with exceptionally high delivery efficiency, 95 %. The 30 % delivery efficiency achieved in the previous study may be attributed to the entrapment of the antibiotic within in the PMVE/MA-PEG 10,000 hydrogel due to hydrogen and ionic bonding. Such observation by which drug molecules remain entrapped with the swollen polymeric network of hydrogel forming MAPs post permeation study has been documented in several of our previous work [21,70]. However, the results presented in the current work revealed that the combination of NS using Soluplus® and dissolving MAPs could potentially enhance the delivery of MTZ into the skin, resulting in high retention of the drug in epidermis and dermis layers, where mostly *B. fragilis* infects, indicated by higher drug extracted compared to MTZ-NS loaded film. The MAPs described here presented a high delivery efficiency. Previous works describing the use of MAPs for NS delivery achieved lower delivery efficiencies (between 7 and 40 %) than the one described here [55,56]. However, it is important to note that these suspensions contained drugs with lower water solubility than MTZ (nestorone and cabotegravir). Moreover, despite the lower drug deposition these MAPs showed clinically relevant plasma drug levels during *in vivo* experiments.

3.7. In vitro antibacterial activity of MTZ-NS loaded MAP

The antimicrobial effect of MAPs loaded with MTZ-NS was tested on cultures of *B. fragilis*. Although, this bacterial species is substantially surpassed by other *Bacteroides* species in the normal bowel microbiota, *B. fragilis* is typically associated with SSTIs [6]. Moreover, *B. fragilis* is one of the most common anaerobic microorganisms found in bacteraemia [71]. The results of the diffusion test are presented in the Fig. 12. MTZ-NS-loaded MAPs displayed a clear and noticeable zone of inhibition which is evidenced from the absence of any *B. fragilis* growth in the entire plate with a zone area of 56.7 ± 0.0 cm^2 ($n \geq 4$), which equates to a circle with a diameter of 8.5 ± 0.0 cm ($n \geq 4$), as can be observed in the Fig. 12. However, as might be expected, the blank MAPs containing only Soluplus® had no zones of inhibition. Moreover, as noted in the Fig. 12, this strain showed a normal bacterial growth. The shadow displayed in the plates containing both type of MAPs (with and without the MTZ-NS) is related to the MAP composition. The dissolving MAPs were fabricated from PVP, glycerol (baseplate) and Soluplus® (tips), thus, when these polymers come into contact with plates, the components of the formulation will start to dissolve forming the transparent zone observed on the top of the plates which contain MAPs. However, these zones should not be confused with a zone of inhibition, since the bacterial growth observed in the plates containing blank MAPs was quite obvious, and different to the polymer dissolution zones. The drug content of each MAP is around 1.85 mg; however, the minimum inhibitory concentrations (MICs) to MTZ among bacteria belonging to the *B. fragilis* group have been reported to range from ≤ 8 µg/ml to ≥ 16 µg/ml for sensitive and resistant strains, respectively [72]. Therefore, it can be postulated that the amount of drug loaded into the MAPs, and the previous reported MICs values would explain the high inhibition exhibited by the MTZ-NS-loaded MAPs.

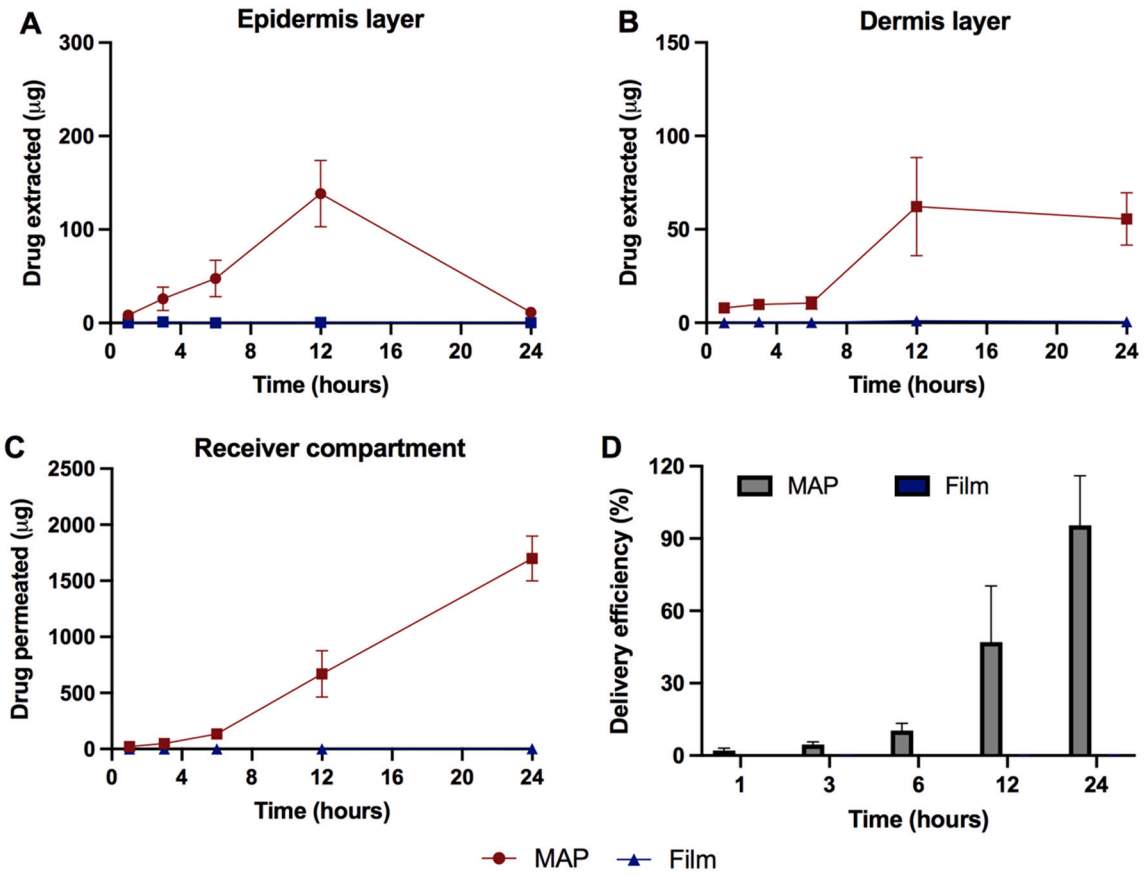

Fig. 11. Amount of metronidazole (MTZ) extracted from (A) epidermis and (B) dermis of excised neonatal porcine skin. (C) Amount of MTZ permeated into the receiver compartment of Franz cells. (values represent means ± SEM, $n = 4$). (D) The delivery efficiency amount of MTZ delivered from MTZ-NS dissolving MAP over the course of 24 h. The film group has been included as a control relative to MAP to demonstrate the need to load the load the drug into an MAP system.

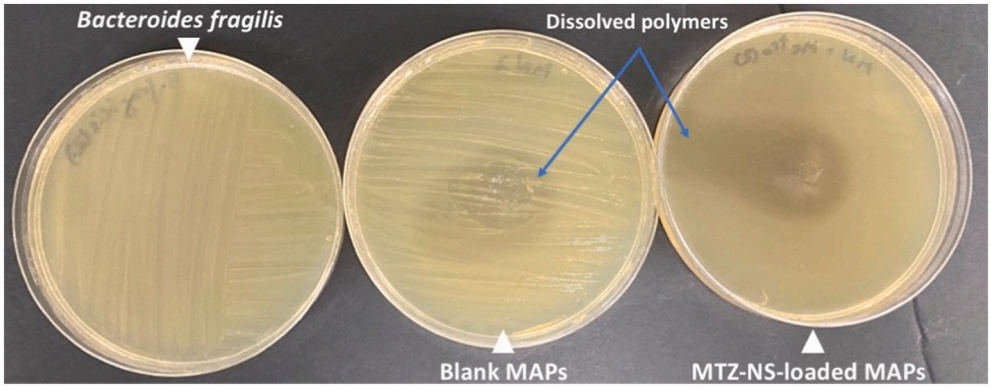

Fig. 12. Representative image showing the inhibition obtained for *B. fragilis* in BHI agar using MTZ-NS-loaded dissolving MAPs (n ≥ 4).

4. Conclusion

The current work highlights the fabrication and evaluation of MTZ-NS loaded dissolving MAPs for the treatment of SSTI. MTT and cell proliferation assays along with LIVE/DEAD™ staining on 3T3L1 cell line showed that the NS was biocompatible with minimal cytotoxicity. Dermatokinetic studies using full thickness *ex vivo* neonatal porcine skin, showed that the MTZ-NS loaded MAPs were able to deliver the antibiotic across all the layers of the skin, resulting in a high delivery efficiency. Lastly, an agar plating assay using bacterial cultures of *B. fragilis* demonstrated that MTZ-NS loaded MAPs resulted in complete bacterial inhibition within the entire plate relative to the control group. Overall, the drug delivery system developed in the current work could provide minimally invasive delivery strategy for MTZ to manage deep rooted SSTIs caused by *B. fragilis* without the need of oral antibiotics therapy or invasive IV infusion. Based on this promising results, future works including *in vivo* efficacy studies must now be done to completely evaluate the therapeutic efficacy of this composite pharmaceutical system in animal models of SSTIs.

CRediT authorship contribution statement

Qonita Kurnia Anjani: Conceptualization, Methodology, Visualization, Investigation, Validation, Formal analysis, Data curation,

Writing – original draft, Writing – review & editing. **Akmal Hidayat Bin Sabri:** Conceptualization, Visualization, Writing – original draft, Writing – review & editing. **Juan Domínguez-Robles:** Methodology, Investigation, Writing – review & editing. **Natalia Moreno-Castellanos:** Methodology, Investigation, Writing – review & editing. **Luki Ahmadi Hari Wardoyo:** Visualization. **Eneko Larrañeta:** Resources, Writing – review & editing. **Ryan F. Donnelly:** Resources, Writing – review & editing, Supervision, Funding acquisition.

Declaration of competing interest

The authors declare that they have no known competing financial interests or personal relationships that could have appeared to influence the work reported in this paper.

Data availability

Data will be made available on request.

Appendix A. Supplementary data

Supplementary data to this article can be found online at https://doi.org/10.1016/j.bioadv.2022.213073.

References

[1] L.G. Miller, D.F. Eisenberg, H. Liu, C.L. Chang, Y. Wang, R. Luthra, A. Wallace, C. Fang, J. Singer, J.A. Suaya, Incidence of skin and soft tissue infections in ambulatory and inpatient settings, 2005–2010, BMC Infect. Dis. 15 (2015) 1–8, https://doi.org/10.1186/s12879-015-1071-0.

[2] K.P. Abhilash, S. Varghese, Profile and outcome of patients presenting with skin and soft-tissue infections to the emergency department, Curr.Med.Issues 17 (2019) 30, https://doi.org/10.4103/cmi.cmi_22_19.

[3] K. Vincent, C. Rotstein, Bacterial skin and soft tissue infections in adults: a review of their epidemiology, pathogenesis, diagnosis, treatment and site of care, Can. J. Infect. Dis. Med. Microbiol. 19 (2008) 173–184.

[4] S. Guégan, F. Lanternier, C. Rouzaud, N. Dupin, O. Lortholary, Fungal skin and soft tissue infections, Curr. Opin. Infect. Dis. 29 (2016) 124–130, https://doi.org/10.1097/QCO.0000000000000252.

[5] M.S. Dryden, Complicated skin and soft tissue infection, J. Antimicrob. Chemother. 65 (2010) 35–44, https://doi.org/10.1093/jac/dkq302.

[6] H.M. Wexler, Bacteroides: the good, the bad, and the nitty-gritty, Clin. Microbiol. Rev. 20 (2007) 593–621, https://doi.org/10.1128/CMR.00008-07/ASSET/A8945CAF-EC58-4D08-BCA7-57F8DF57FB99/ASSETS/GRAPHIC/ZCM0040722230003.JPEG.

[7] A. Wanger, V. Chavez, R.S.P. Huang, A. Wahed, J.K. Actor, A. Dasgupta, Overview of Bacteria, Elsevier, 2017, https://doi.org/10.1016/b978-0-12-805351-5.00006-5.

[8] D. Edwards, Mechanisms of selective toxicity of metronidazole and other nitroimidazole drugs, Br. J. Vener. Dis. 56 (1980) 285–290, https://doi.org/10.1136/sti.57.4.279.

[9] NICE Excellence, Metronidazole|Drug|BNF content published by NICE (n.d.). https://bnf.nice.org.uk/drug/metronidazole.html.

[10] M. Brandt, C. Abels, T. May, K. Lohmann, I. Schmidts-Winkler, U.B. Hoyme, Intravaginally applied metronidazole is as effective as orally applied in the treatment of bacterial vaginosis, but exhibits significantly less side effects, Eur.J. Obstet.Gynecol.Reprod.Biol. 141 (2008) 158–162, https://doi.org/10.1016/j.ejogrb.2008.07.022.

[11] S.A. Kelly, A.M. Rodgers, S.C. O'Brien, R.F. Donnelly, B.F. Gilmore, Gut check time: antibiotic delivery strategies to reduce antimicrobial resistance, Trends Biotechnol. 38 (2020) 447–462, https://doi.org/10.1016/j.tibtech.2019.10.008.

[12] P.N. Davies, H.E.C. Worthington, F. Podczeck, J.M. Newton, The determination of the mechanical strength of tablets of different shapes, Eur. J. Pharm. Biopharm. 67 (2007) 268–276, https://doi.org/10.1016/j.ejpb.2007.01.014.

[13] S. Latha, P. Selvamani, C.S. Kumar, P. Sharavanan, G. Suganya, V.S. Beniwal, P. R. Rao, Formulation development and evaluation of metronidazole magnetic nanosuspension as a magnetic-targeted and polymeric-controlled drug delivery system, J. Magn. Magn. Mater. 321 (2009) 1580–1585, https://doi.org/10.1016/J.JMMM.2009.02.089.

[14] N.M. Badawi, M.A. Elkafrawy, R.M. Yehia, D.A. Attia, Clinical comparative study of optimized metronidazole loaded lipid nanocarrier vaginal emulgel for management of bacterial vaginosis and its recurrence, Drug Deliv. 28 (2021) 814–825, https://doi.org/10.1080/10717544.2021.1912211.

[15] M.J. Garland, K. Migalska, T.M. Tuan-Mahmood, T.Raghu Raj Singh, R. Majithija, E. Caffarel-Salvador, C.M. McCrudden, H.O. McCarthy, A.David Woolfson, R. F. Donnelly, Influence of skin model on in vitro performance of drug-loaded soluble microneedle arrays, Int. J. Pharm. 434 (2012) 80–89, https://doi.org/10.1016/J.IJPHARM.2012.05.069.

[16] A.D. Permana, A.J. Paredes, F. Volpe-Zanutto, Q.K. Anjani, E. Utomo, R. F. Donnelly, Dissolving microneedle-mediated dermal delivery of itraconazole nanocrystals for improved treatment of cutaneous candidiasis, Eur. J. Pharm. Biopharm. 154 (2020) 50–61, https://doi.org/10.1016/j.ejpb.2020.06.025.

[17] S. D'Souza, A review of in vitro drug release test methods for nano-sized dosage forms, Adv.Pharm. 2014 (2014) 1–12, https://doi.org/10.1155/2014/304757.

[18] N. Chidambaram, D.J. Burgess, A novel in vitro release method for submicron-sized dispersed systems, AAPS PharmSci. 1 (1999) 32, https://doi.org/10.1208/PS010311.

[19] R.F. Donnelly, M.T.C. McCrudden, A.Z. Alkilani, E. Larrañeta, E. McAlister, A. J. Courtenay, M.C. Kearney, T.R. Raj Singh, H.O. McCarthy, V.L. Kett, E. Caffarel-Salvador, S. Al-Zahrani, A.D. Woolfson, Hydrogel-forming microneedles prepared from "super swelling" polymers combined with lyophilised wafers for transdermal drug delivery, PLoS ONE 9 (2014), https://doi.org/10.1371/journal.pone.0111547.

[20] R.F. Donnelly, T.R.R. Singh, M.J. Garland, K. Migalska, R. Majithiya, C. M. McCrudden, P.L. Kole, T.M.T. Mahmood, H.O. McCarthy, A.D. Woolfson, Hydrogel-forming microneedle arrays for enhanced transdermal drug delivery, Adv. Funct. Mater. 22 (2012) 4879–4890, https://doi.org/10.1002/adfm.201200864.

[21] Q.K. Anjani, A.D. Permana, Á. Cárcamo-Martínez, J. Domínguez-Robles, I. A. Tekko, E. Larrañeta, L.K. Vora, D. Ramadon, R.F. Donnelly, Versatility of hydrogel-forming microneedles in in vitro transdermal delivery of tuberculosis drugs, Eur. J. Pharm. Biopharm. 158 (2021) 294–312, https://doi.org/10.1016/j.ejpb.2020.12.003.

[22] R.F. Donnelly, M.J. Garland, D.I.J. Morrow, K. Migalska, T. Raghu, R. Singh, R. Majithiya, A.D. Woolfson, Optical coherence tomography is a valuable tool in the study of the effects of microneedle geometry on skin penetration characteristics and in-skin dissolution, J. Control. Release 147 (2010) 333–341, https://doi.org/10.1016/j.jconrel.2010.08.008.

[23] Q.K. Anjani, A.H. bin Sabri, E. Utomo, J. Domínguez-Robles, R.F. Donnelly, Elucidating the impact of surfactants on the performance of dissolving microneedle array patches, Mol. Pharm. (2022), https://doi.org/10.1021/ACS.MOLPHARMACEUT.1C00988 acs.molpharmaceut.1c00988.

[24] Y. Sánchez-Cardona, C.E. Echeverri-Cuartas, M.E.L. López, N. Moreno-Castellanos, Chitosan/gelatin/PVA scaffolds for beta pancreatic cell culture, Polymers 13 (2021) 2372, https://doi.org/10.3390/POLYM13142372, 2021, Vol. 13, Page 2372.

[25] Á. Cárcamo-Martínez, B. Mallon, Q.K. Anjani, J. Domínguez-Robles, E. Utomo, L. K. Vora, I.A. Tekko, E. Larrañeta, R.F. Donnelly, Enhancing intradermal delivery of tofacitinib citrate: comparison between powder-loaded hollow microneedle arrays and dissolving microneedle arrays, Int. J. Pharm. 593 (2021), https://doi.org/10.1016/j.ijpharm.2020.120152.

[26] C. Knieke, M. Sommer, W. Peukert, Identifying the apparent and true grinding limit, Powder Technol. 195 (2009) 25–30, https://doi.org/10.1016/j.powtec.2009.05.007.

[27] L. Peltonen, Design space and QbD approach for production of drug nanocrystals by wet media milling techniques, Pharmaceutics 10 (2018), https://doi.org/10.3390/pharmaceutics10030104.

[28] F. Al-Akayleh, I. Al-Naji, S. Adwan, M. Al-Remawi, M. Shubair, Enhancement of curcumin solubility using a novel solubilizing polymer Soluplus®, J. Pharm. Innov. 17 (2022) 142–154, https://doi.org/10.1007/s12247-020-09500-x.

[29] L. Peltonen, J. Hirvonen, Pharmaceutical nanocrystals by nanomilling: critical process parameters, particle fracturing and stabilization methods, J. Pharm. Pharmacol. 62 (2010) 1569–1579, https://doi.org/10.1111/j.2042-7158.2010.01022.x.

[30] P. Liu, T. Viitala, A. Kartal-Hodzic, H. Liang, T. Laaksonen, J. Hirvonen, L. Peltonen, Interaction studies between indomethacin nanocrystals and PEO/PPO copolymer stabilizers, Pharm. Res. 32 (2015) 628–639, https://doi.org/10.1007/s11095-014-1491-3.

[31] B. Van Eerdenbrugh, G. Van den Mooter, P. Augustijns, Top-down production of drug nanocrystals: nanosuspension stabilization, miniaturization and transformation into solid products, Int. J. Pharm. 364 (2008) 64–75, https://doi.org/10.1016/j.ijpharm.2008.07.023.

[32] Y. Dong, H. Zhu, Y. Shen, W. Zhang, L. Zhang, Antibacterial activity of silver nanoparticles of different particle size against Vibrio natriegens, PLoS ONE 14 (2019), https://doi.org/10.1371/JOURNAL.PONE.0222322.

[33] M. Inam, J.C. Foster, J. Gao, Y. Hong, J. Du, A.P. Dove, R.K. O'Reilly, Size and shape affects the antimicrobial activity of quaternized nanoparticles, J. Polym. Sci. A Polym. Chem. 57 (2019) 255–259, https://doi.org/10.1002/POLA.29195.

[34] Q.K. Anjani, A.D. Permana, Á. Cárcamo-Martínez, J. Domínguez-Robles, I. A. Tekko, E. Larrañeta, L.K. Vora, D. Ramadon, R.F. Donnelly, Versatility of hydrogel-forming microneedles in in vitro transdermal delivery of tuberculosis drugs, Eur. J. Pharm. Biopharm. 294–312 (2021) 294–312, https://doi.org/10.1016/j.ejpb.2020.12.003.

[35] A.D. Permana, I.A. Tekko, M.T.C. McCrudden, Q.K. Anjani, D. Ramadon, H. O. McCarthy, R.F. Donnelly, Solid lipid nanoparticle-based dissolving microneedles: a promising intradermal lymph targeting drug delivery system with potential for enhanced treatment of lymphatic filariasis, J. Control. Release 316 (2019) 34–52, https://doi.org/10.1016/j.jconrel.2019.10.004.

[36] A. Karakucuk, N. Celebi, Investigation of formulation and process parameters of wet media milling to develop etodolac nanosuspensions, Pharm. Res. 37 (2020) 1–18, https://doi.org/10.1007/S11095-020-02815-X/FIGURES/13.

[37] M.H. Shariare, M.A. Altamimi, A.L. Marzan, R. Tabassum, B. Jahan, H.M. Reza, M. Rahman, G.U. Ahsan, M. Kazi, In Vitro Dissolution and Bioavailability Study of

Furosemide Nanosuspension Prepared Using Design of Experiment (DoE), 2019, https://doi.org/10.1016/j.jsps.2018.09.002.
[38] B.Y. Gajera, D.A. Shah, R.H. Dave, Development of an amorphous nanosuspension by sonoprecipitation-formulation and process optimization using design of experiment methodology, Int. J. Pharm. 559 (2019) 348–359, https://doi.org/10.1016/J.IJPHARM.2019.01.054.
[39] M. Colombo, S. Orthmann, M. Bellini, S. Staufenbiel, R. Bodmeier, Influence of drug brittleness, nanomilling time, and freeze-drying on the crystallinity of poorly water-soluble drugs and its implications for solubility enhancement, AAPS PharmSciTech 18 (2017) 2437–2445, https://doi.org/10.1208/S12249-017-0722-4/FIGURES/7.
[40] L. Peltonen, J. Hirvonen, Pharmaceutical nanocrystals by nanomilling: critical process parameters, particle fracturing and stabilization methods, J. Pharm. Pharmacol. 62 (2010) 1569–1579, https://doi.org/10.1111/J.2042-7158.2010.01022.X.
[41] A.D. Permana, A.J. Paredes, F.V. Zanutto, M.N. Amir, I. Ismail, M.A. Bahar, S. D. Sumarheni, R.F.Donnelly Palma, Albendazole nanocrystal-based dissolving microneedles with improved pharmacokinetic performance for enhanced treatment of cystic echinococcosis, ACS Appl. Mater. Interfaces 13 (2021) 38745–38760, https://doi.org/10.1021/ACSAMI.1C11179/ASSET/IMAGES/MEDIUM/AM1C11179_0012.GIF.
[42] C. Bartos, O. Jójárt-Laczkovich, G. Katona, M. Budai-Szűcs, R. Ambrus, A. Bocsik, I. Gróf, M.A. Deli, P. Szabó-Révész, Optimization of a combined wet milling process in order to produce poly(vinyl alcohol) stabilized nanosuspension, Drug Des.Dev. Ther. 12 (2018) 1567–1580, https://doi.org/10.2147/DDDT.S159965.
[43] V. Mokale, K. Patil, T. Khatik, Y. Sutar, Glyburide nanosuspension: influence of processing and formulation parameter on solubility and in vitro dissolution behavior, <sb:contribution><sb:title>Asian</sb:title></sb:contribution><sb:host><sb:issue><sb:series><sb:title>J. Pharm.</sb:title></sb:series></sb:issue></sb:host> 7 (2013) 111–117, https://doi.org/10.4103/0973-8398.120085.
[44] E. Larrañeta, J. Moore, E.M. Vicente-Pérez, P. González-Vázquez, R. Lutton, A. D. Woolfson, R.F. Donnelly, A proposed model membrane and test method for microneedle insertion studies, Int. J. Pharm. 472 (2014) 65–73, https://doi.org/10.1016/j.ijpharm.2014.05.042.
[45] F. Siepmann, V. le Brun, J. Siepmann, Drugs acting as plasticizers in polymeric systems: a quantitative treatment, J. Control. Release 115 (2006) 298–306, https://doi.org/10.1016/J.JCONREL.2006.08.016.
[46] I.A. Tekko, L.K. Vora, F. Volpe-zanutto, K. Moffatt, C. Jarrahian, H.O. Mccarthy, R. F. Donnelly, Novel bilayer microarray patch-assisted long-acting micro-depot cabotegravir intradermal delivery for HIV pre-exposure prophylaxis, Adv. Funct. Mater. 32 (2022) 2106999, https://doi.org/10.1002/adfm.202106999.
[47] A.D. Permana, A.J. Paredes, F. Volpe-Zanutto, Q.K. Anjani, E. Utomo, R. F. Donnelly, Dissolving microneedle-mediated dermal delivery of itraconazole nanocrystals for improved treatment of cutaneous candidiasis, Eur. J. Pharm. Biopharm. 154 (2020) 50–61, https://doi.org/10.1016/j.ejpb.2020.06.025.
[48] T. Nakatsuji, H. Chiang, S.B. Jiang, H. Nagarajan, K. Zengler, R.L. Gallo, The microbiome extends to subepidermal compartments of normal skin, <sb:contribution><sb:title>Nat. </sb:title></sb:contribution><sb:host><sb:issue><sb:series><sb:title>Commun. </sb:title></sb:series></sb:issue></sb:host> (2013) 1–8, https://doi.org/10.1038/ncomms2441.
[49] M. Kirkby, A.B. Sabri, D.J. Scurr, G.P. Moss, Dendrimer-mediated permeation enhancement of chlorhexidine digluconate: determination of in vitro skin permeability and visualisation of dermal distribution, Eur. J. Pharm. Biopharm. 159 (2021) 77–87, https://doi.org/10.1016/j.ejpb.2020.12.014.
[50] E. Altuntaş, I.A. Tekko, L.K. Vora, N. Kumar, R. Brodsky, O. Chevallier, E. McAlister, Q. Kurnia Anjani, H.O. McCarthy, R.F. Donnelly, Nestorone nanosuspension-loaded dissolving microneedles array patch: a promising novel approach for “on-demand” hormonal female-controlled peritcoital contraception, Int. J. Pharm. 614 (2022), 121422, https://doi.org/10.1016/J.IJPHARM.2021.121422.
[51] I.A. Tekko, A.D. Permana, L. Vora, T. Hatahet, H.O. McCarthy, R.F. Donnelly, Localised and sustained intradermal delivery of methotrexate using nanocrystal-loaded microneedle arrays: potential for enhanced treatment of psoriasis, Eur. J. Pharm. Sci. 152 (2020), 105469, https://doi.org/10.1016/J.EJPS.2020.105469.
[52] M.T.C. Mc Crudden, E. Larrañeta, A. Clark, C. Jarrahian, A. Rein-Weston, B. Creelman, Y. Moyo, S. Lachau-Durand, N. Niemeijer, P. Williams, H. O. McCarthy, D. Zehrung, R.F. Donnelly, Design, formulation, and evaluation of novel dissolving microarray patches containing rilpivirine for intravaginal delivery, Adv.Healthc.Mater. 8 (2019) 1801510, https://doi.org/10.1002/ADHM.201801510.
[53] M.T.C. Mc Crudden, E. Larrañeta, A. Clark, C. Jarrahian, A. Rein-Weston, S. Lachau-Durand, N. Niemeijer, P. Williams, C. Haeck, H.O. McCarthy, D. Zehrung, R.F. Donnelly, Design, formulation and evaluation of novel dissolving microarray patches containing a long-acting rilpivirine nanosuspension, J. Control. Release 292 (2018) 119–129, https://doi.org/10.1016/J.JCONREL.2018.11.002.
[54] S. Abdelghany, I.A. Tekko, L. Vora, E. Larrañeta, A.D. Permana, R.F. Donnelly, Nanosuspension-based dissolving microneedle arrays for intradermal delivery of curcumin, Pharmaceutics 11 (2019) 308, https://doi.org/10.3390/PHARMACEUTICS11070308, 2019, Vol. 11, Page 308.
[55] I.A. Tekko, L.K. Vora, F. Volpe-Zanutto, K. Moffatt, C. Jarrahian, H.O. Mccarthy, R. F. Donnelly, I.A. Tekko, L.K. Vora, F. Volpe-Zanutto, K. Moffatt, H.O. Mccarthy, R. F. Donnelly, Novel bilayer microarray patch-assisted long-acting micro-depot cabotegravir intradermal delivery for HIV pre-exposure prophylaxis, Adv. Funct. Mater. 32 (2022), 2106999, https://doi.org/10.1002/ADFM.202106999.
[56] E. Altuntaş, I.A. Tekko, L.K. Vora, N. Kumar, R. Brodsky, O. Chevallier, E. McAlister, Q. Kurnia Anjani, H.O. McCarthy, R.F. Donnelly, Nestorone nanosuspension-loaded dissolving microneedles array patch: a promising novel approach for “on-demand” hormonal female-controlled peritcoital contraception, Int. J. Pharm. 614 (2022), 121422, https://doi.org/10.1016/J.IJPHARM.2021.121422.
[57] A.T. Ogunjimi, J. Carr, C. Lawson, N. Ferguson, N.K. Brogden, Micropore closure time is longer following microneedle application to skin of color, Sci. Rep. 10 (2020) 1–14, https://doi.org/10.1038/s41598-020-75246-8, 2020 10:1.
[58] Y.C. Kim, J.H. Park, M.R. Prausnitz, Microneedles for drug and vaccine delivery, Adv. Drug Deliv. Rev. 64 (2012) 1547, https://doi.org/10.1016/J.ADDR.2012.04.005.
[59] A.H. Sabri, J. Ogilvie, K. Abdulhamid, V. Shpadaruk, J. McKenna, J. Segal, D. J. Scurr, M. Marlow, Expanding the applications of microneedles in dermatology, Eur. J. Pharm. Biopharm. 140 (2019) 121–140, https://doi.org/10.1016/J.EJPB.2019.05.001.
[60] E. McAlister, B. Dutton, L.K. Vora, L. Zhao, A. Ripolin, D.S.Z.B.P.H. Zahari, H. L. Quinn, I.A. Tekko, A.J. Courtenay, S.A. Kelly, A.M. Rodgers, L. Steiner, G. Levin, E. Levy-Nissenbaum, N. Shterman, H.O. McCarthy, R.F. Donnelly, Directly compressed tablets: a novel drug-containing reservoir combined with hydrogel-forming microneedle arrays for transdermal drug delivery, Adv.Healthc.Mater. 10 (2021) 2001256, https://doi.org/10.1002/ADHM.202001256.
[61] A.H. bin Sabri, Q.K. Anjani, E. Utomo, A. Ripolin, R.F. Donnelly, Development and characterization of a dry reservoir-hydrogel-forming microneedles composite for minimally invasive delivery of cefazolin, Int. J. Pharm. 617 (2022) 121593, https://doi.org/10.1016/J.IJPHARM.2022.121593.
[62] R.F. Donnelly, R.R.S. Thakur, M.J. Garland, K. Migalska, R. Majithiya, C. M. McCrudden, P.L. Kole, T.M.T. Mahmood, H.O. McCarthy, A.D. Woolfson, T.R. R. Singh, M.J. Garland, K. Migalska, R. Majithiya, C.M. McCrudden, P.L. Kole, T.M. T. Mahmood, H.O. McCarthy, A.D. Woolfson, Hydrogel-forming microneedle arrays for enhanced transdermal drug delivery, Adv. Funct. Mater. 22 (2012) 4879–4890, https://doi.org/10.1002/adfm.201200864.
[63] J.F. Alopaeus, E. Hagesæther, I. Tho, Micellisation mechanism and behaviour of Soluplus®–furosemide micelles: preformulation studies of an oral nanocarrier-based system, Pharmaceuticals 12 (2019) 15, https://doi.org/10.3390/PH12010015, 2019, Vol. 12, Page 15.
[64] S. Patnaik, L.A.A. Chunduri, M.S. Akilesh, S.S. Bhagavatham, V. Kamisetti, in: Enhanced Dissolution Characteristics of Piroxicam–Soluplus® Nanosuspensions 11, 2016, pp. 916–929, https://doi.org/10.1080/17458080.2016.1178402.
[65] L.C.T. Trindade, J.E.F. Matias, C.P.P.S. Aio, R.E. Farias, M.D.L.P. Biondo-Simões, Differentiation of myofibroblasts in wounds after topical use of metronidazole: an experimental study, Rev.Colegio Bras.Cirurgioes 46 (2019), https://doi.org/10.1590/0100-6991E-20192015.
[66] K. Dua, V.R. Malipeddi, J. Madan, G. Gupta, S. Chakravarthi, R. Awasthi, I. S. Kikuchi, T.J.A. de Pinto, Norfloxacin and metronidazole topical formulations for effective treatment of bacterial infections and burn wounds, interventional medicine and appliedScience 8 (2016) 68–76, https://doi.org/10.1556/1646.8.2016.2.4.
[67] A.A. El-Shanshory, M.M. Agwa, A.I. Abd-Elhamid, H.M.A. Soliman, X. Mo, E. R. Kenawy, Metronidazole topically immobilized electrospun nanofibrous scaffold: novel secondary intention wound healing accelerator, Polymers (Basel) 14 (2022), https://doi.org/10.3390/polym14030454.
[68] K. Peng, L.K. Vora, I.A. Tekko, A. Dian, J. Domínguez-, D. Ramadon, P. Chambers, H.O. Mccarthy, E. Larra, F. Donnelly, Dissolving microneedle patches loaded with amphotericin B microparticles for localised and sustained intradermal delivery: potential for enhanced treatment of cutaneous fungal infections, J. Control. Release 339 (2021) 361–380, https://doi.org/10.1016/j.jconrel.2021.10.001.
[69] N.M. Mahfouz, M.A. Hassan, Synthesis, chemical and enzymatic hydrolysis, and bioavailability evaluation in rabbits of metronidazole amino acid ester prodrugs with enhanced water solubility, J. Pharm. Pharmacol. (2001) 841–848, https://doi.org/10.1211/0022357011776199.
[70] A.H. Bin Sabri, Q.K. Anjani, E. Utomo, A. Ripolin, R.F. Donnelly, Development and characterization of a dry reservoir-hydrogel-forming microneedles composite for minimally invasive delivery of cefazolin, Int. J. Pharm. 617 (2022), 121593, https://doi.org/10.1016/j.ijpharm.2022.121593.
[71] E.J.C. Goldstein, D.M. Citron, Activity of a novel carbapenem, doripenem, against anaerobic pathogens, Diagn. Microbiol. Infect. Dis. 63 (2009) 447–454, https://doi.org/10.1016/J.DIAGMICROBIO.2009.01.022.
[72] Y. Shafquat, K. Jabeen, J. Farooqi, K. Mehmood, S. Irfan, R. Hasan, A. Zafar, Antimicrobial susceptibility against metronidazole and carbapenem in clinical anaerobic isolates from Pakistan, antimicrobial resistance and infectionControl 8 (2019) 1–7, https://doi.org/10.1186/S13756-019-0549-8/TABLES/3.